NAVAL POSTGRADUATE SCHOOL
Monterey, California

THESIS

TRANSONIC COMPRESSOR TEST RIG REBUILD AND INITIAL RESULTS WITH THE SANGER STAGE

by

Joseph Morton O'Brien

June 2000

Thesis Advisor: Raymond Shreeve

Approved for public release; distribution is unlimited.

20000823 049

REPORT DOCUMENTATION PAGE

Form Approved
OMB No. 0704-0188

1. AGENCY USE ONLY *(Leave blank)*	2. REPORT DATE June 2000	3. REPORT TYPE AND DATES COVERED Master's Thesis

4. TITLE AND SUBTITLE Transonic Compressor Test Rig Rebuild and Initial Results with the Sanger Stage	5. FUNDING NUMBERS
6. AUTHOR(S) O'Brien, Joseph Morton	

7. PERFORMING ORGANIZATION NAME(S) AND ADDRESS(ES) Naval Postgraduate School Monterey, CA 93943-5000	8. PERFORMING ORGANIZATION REPORT NUMBER

9. SPONSORING / MONITORING AGENCY NAME(S) AND ADDRESS(ES) Naval Air Warfare Center Aircraft Division	10. SPONSORING / MONITORING AGENCY REPORT NUMBER

11. SUPPLEMENTARY NOTES

The views expressed in this thesis are those of the author and do not reflect the official policy or position of the Department of Defense or the U.S. Government.

12a. DISTRIBUTION / AVAILABILITY STATEMENT Approved for public release; distribution is unlimited.	12b. DISTRIBUTION CODE

13. ABSTRACT *(maximum 200 words)*

The NPS Transonic Compressor Test Rig was rebuilt and initial testing was conducted on the Sanger Stage, which was designed using CFD techniques. Improvements to the existing monitoring equipment, test rig instrumentation, and data acquisition software were all made in preparation for testing. A Plexiglas casewall was chosen to accommodate pressure-sensitive paint measurements. Wall heating was used to control tip-clearance. The initial performance data, to 70% design speed, were compared with predictions using a 3-dimensional viscous code.

14. SUBJECT TERMS Compressor, Transonic, CFD, Turbomachinery, Tip Clearance	15. NUMBER OF PAGES 110
	16. PRICE CODE

17. SECURITY CLASSIFICATION OF REPORT Unclassified	18. SECURITY CLASSIFICATION OF THIS PAGE Unclassified	19. SECURITY CLASSIFI- CATION OF ABSTRACT Unclassified	20. LIMITATION OF ABSTRACT UL

TRANSONIC CMPRESSOR TEST RIG REBUILD AND INITIAL RESULTS WITH THE SANGER STAGE

Joseph M. O'Brien
Ensign, United States Navy
B.S., United States Naval Academy, 1999

Submitted in partial fulfillment of the
requirements for the degree of

MASTER OF SCIENCE IN AERONAUTICAL ENGINEERING

from the

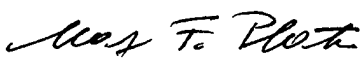## NAVAL POSTGRADUATE SCHOOL
June 2000

Author: _____
Joseph Morton O'Brien

Approved by: _____
Raymond Shreeve, Thesis Advisor

_____
Garth Hobson, Second Reader

_____
Maximilian F. Platzer, Chairman
Department of Aeronautics and Astronautics

iv

ABSTRACT

The NPS Transonic Compressor Test Rig was rebuilt and initial testing was conducted on the Sanger Stage, which was designed using CFD techniques. Improvements to the existing monitoring equipment, test rig instrumentation, and data acquisition software were all made in preparation for testing. A Plexiglas casewall was chosen to accommodate pressure-sensitive paint measurements. Wall heating was used to control tip-clearance. The initial performance data, to 70% design speed, were compared with predictions using a 3-dimensional viscous code.

TABLE OF CONTENTS

LIST OF FIGURES

LIST OF TABLES

ACKNOWLEDGMENTS

I.   INTRODUCTION

A transonic axial compressor stage was designed by Nelson L. Sanger [Ref. 1] in 1994, at the NASA Lewis Research Center for the Naval Postgraduate School to evaluate in the Transonic Compressor Rig (TCR). The failure of a spinner retaining bolt in 1997, during testing at 80% of design speed [Ref. 2], resulted in a loss of the initial Sanger stage. Testing was being conducted to determine the performance of the stage, for eventual comparison with CFD predictions.

In the present work, the stage was remanufactured, the test rig was reconstructed and reinstrumented, and improvements were made to the data acquisition hardware and software. Improvements were also made in the operating controls and monitoring equipment. Performance testing was then conducted at 50, 60 and 70 percent of design speed. Testing was halted at 70% speed after it was found that the temperature of the Plexiglas casewall had a major impact on the size of the tip clearance gap. It was demonstrated that wall heating could be used to control the tip clearance.

The present report documents the rebuilding of the Transonic Compressor Rig and the replacement and improvement of its instrumentation, the testing of the Sanger stage, and the discoveries made on the effects of casewall temperature on tip clearance.

THIS PAGE INTENTIONALLY LEFT BLANK

II.   TEST RIG AND INSTRUMENTATION

A.   HARDWARE DESCRIPTION

1.   Transonic Compressor Rig

The general layout of the Transonic Compressor Rig (TCR) within the high-speed turbopropulsion facility is shown in Fig. 1. The test compressor was driven by two opposed-rotor air turbine stages, supplied by a 12-stage Allis-Chalmers axial compressor. The Allis-Chalmers compressor was capable of supplying air pressure up to 30 pounds per square inch gauge, at a flow rate of up to 11 pounds per second. Air from the compressor was fed through a motor-driven valve into the turbine drive unit which was adjusted manually to control the speed of the compressor. Air from the atmosphere entered via a throttle valve into the settling chamber, entered the rotor axially, and was fed through a honeycomb straightener located behind the stator, before being vented from the test compressor.

A second, high pressure compressor, capable of providing up to 150 pounds per square inch gauge, was used to provide air to a balance piston located on the drive shaft, which controlled the axial force on the bearings in the rotor assembly. A third shop compressor was used to provide dry air for the bearing oil-mist lubrication system, and other instrument air requirements.
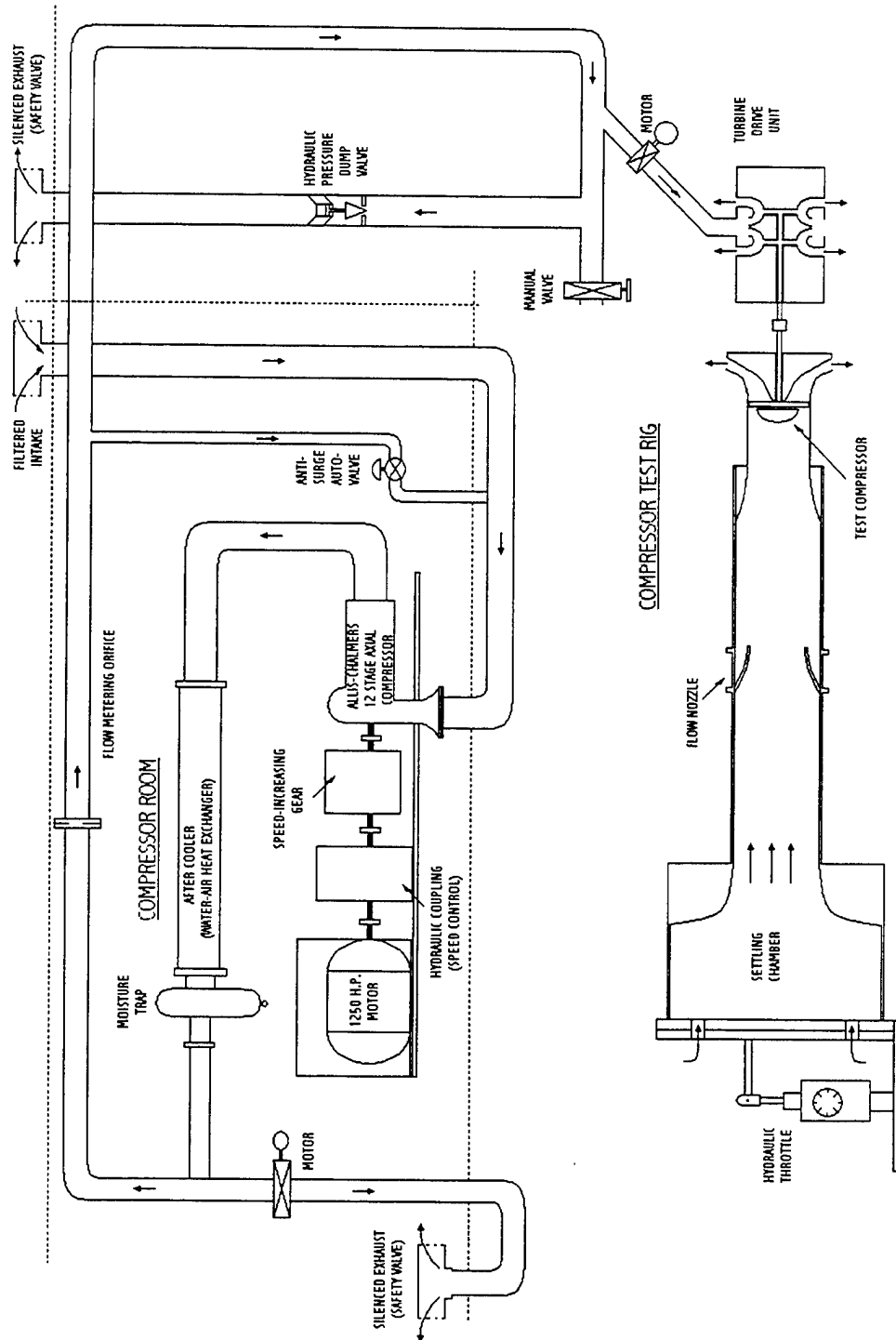
Figure 1.   Schematic of the Facility

4

2. Casewall

A new casewall was installed for the present test program. Figure 2 shows the casewall before and after installation respectively. The casing had provisions for pressure and temperature probes to be located before, aft, and between the rotor and stator. The casewall was made of Plexiglas (type UVT), and was the same design as the previous Lucite casing [Ref. 2]. However, the previous casewall had a larger inner diameter. The tip clearance was a major concern in the design and installation of the new casewall. The static tip gap clearance was intended to be 0.09 inches, and the expected design speed running clearance to be 0.004 inches. The transparency of the casewall allowed visual and remote video observations of the operating stage, and was intended for the future use of optical measuring methods such as pressure-sensitive paint.

B. OPERATING CONTROLS AND INSTRUMENTATION

The TCR was operated under manual control from a control room outside the compressor test cell. A photograph of the console is shown in Fig. 3. An electrically actuated butterfly valve was used to control the speed of the turbine drive unit. A rotating-plate throttle was used to regulate the air flow through the compressor. These two controls allowed test data to be acquired to define a constant speed line on a compressor map. The axial force on the rotor was maintained near zero at all times by adjusting the balance-piston air and monitoring a strain gauge panel meter. Bearing temperatures were monitored using J-type thermocouples (Fig. 4) that were located
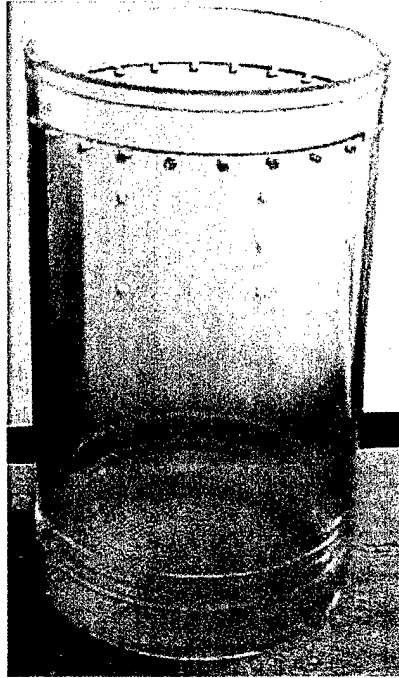
(a)
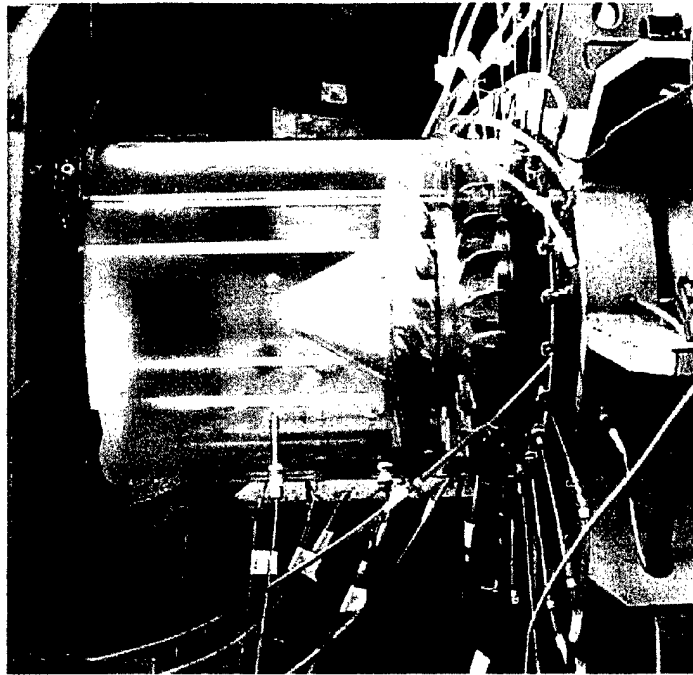
(b)

Figure 2.   Casewall Prior to (a) and After (b) Assembly

Figure 3.   Photograph of the Control Console

against the outer races of the eight bearings supporting the turbine and test compressor drive shafts.

Figure 4.   Type J Thermocouple For Sensing Bearing Temperature

The speed of the Allis-Chalmer compressor was also monitored, since fast changes in load on the compressor could overcome the speed control. An emergency dump valve was available to unload the drive turbine and prevent overspeeding the compressor.

The parameters monitored at the control console were not used in the data reduction and were not automatically recorded during test runs. They were used to set and monitor the test conditions, and to operate safely. The calibration of the instrumentation used to monitor the operation is described in Appendix B.

8

C. SANGER STAGE AND INSTRUMENTATION

1. Sanger Stage

Figure 5 is a sectioned view of the Sanger stage, and its assembly in the transonic compressor test rig. The figure also shows the measurement stations in the flow, with station one being in front of the rotor, station two between the rotor and the stator, and station three aft of the stator. Figure 6 shows the rotor and stator mounted on the TCR. The stage consisted of a rotor with 22 blades, and a stator with 27 blades. Table 1 provides the design specifications for the Sanger stage. An analysis of the rotor modal response was conducted to compare measured frequencies with those found using a Finite Element analysis (Appendix A). Determining these primary frequencies was necessary to determine ranges of resonant speed to avoid while testing of the stage.

Parameter	Final Selection
Rotor Pressure Ratio	1.61
Stage Pressure Ratio	1.56
Tip Speed	1300 ft/sec
Design Speed	27085 rpm
Design Mass Flow	17.05 lb/s
Specific Mass Flow	35 lbm/sec-ft^2
Specific Head Rise	0.246
Tip Inlet Relative Mach Number	1.28
Hub/Tip Radius Ratio	0.51
Rotor Inlet Ramp Angle	28.2 degrees
Power Required	457 HP

Table 1.   Design Parameters for the Sanger Stage
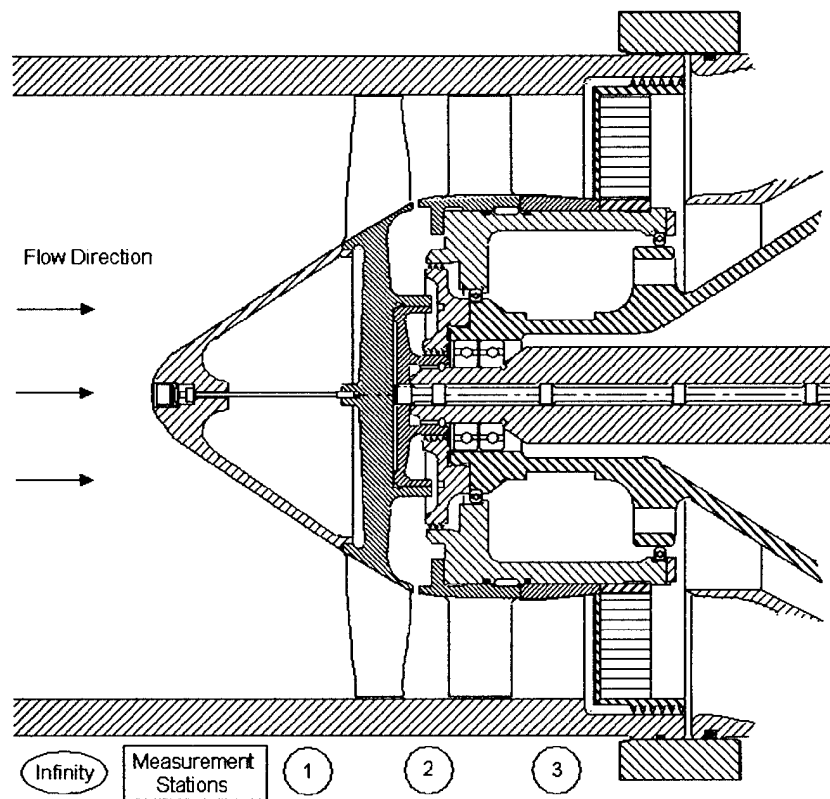
Figure 5.   Sectioned view of the Sanger Stage in the Test Rig After Ref. 3
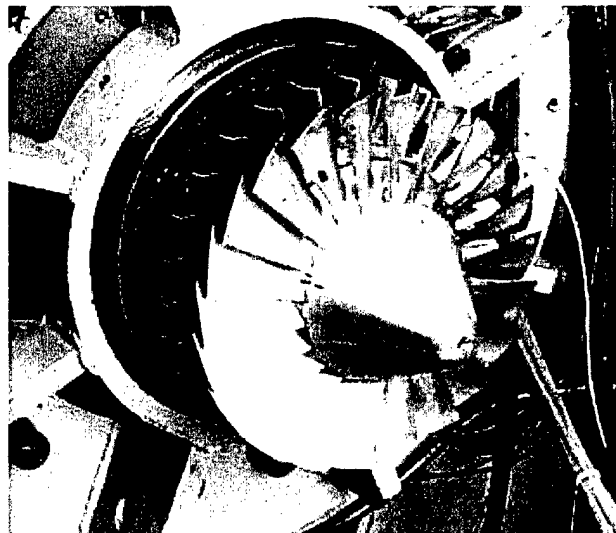
Figure 6.   Rotor-Stator Assembly Prior to Casewall Installation

2. Measurement Devices

The instrumentation for measuring stage performance, included static pressure taps, Kiel pressure probes, Kiel/thermocouple combination probes, a torque measurement system, a mass flow rate measurement system, and a magnetic speed pickup. Two types of Kiel probes were used; a 1/16 inch "Miniature Head" Kiel Probe (United Sensor KAA-8, [Ref 4]) and a 1/8 inch "Standard Head" combination Kiel/thermocouple Probe (United Sensor KT-8-J-12-C, [Ref. 4]).
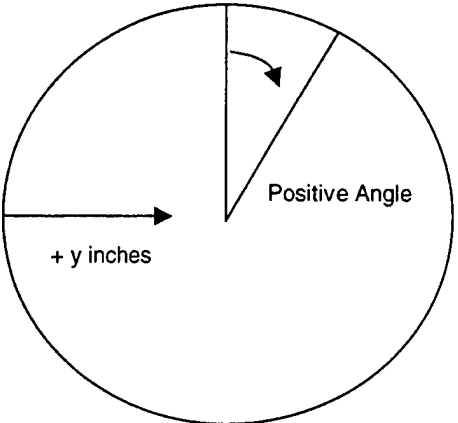
The static pressure ports were 1/32 inch taps located at various locations along the casewall, and in the hub of the stator at measurement stations two and three. Table 3 gives the locations of the various total and static pressure measurements, and their corresponding Scanivalve port assignments.

A cantilevered flexure was used to measured the torque on the stator. Four strain gauges on the flexure provided a near linear response to bending. Appendix B details the calibration of the torque measurement system. A magnetic flux cutter and a disk with six holes mounted on the shaft of the drive turbine, was used to measure the rotational speed of the rotor. The pressure differential across the nozzle, was recorded and used in the measurement of the mass flow rate. This pressure differential was also monitored in the control room using a water manometer, in order to set increments of flow rate.

At measurement station 1, two combination probes were set 2 inches from the inner wall of the casing to measure inlet total pressure and temperature. Twenty three (23) ports located at station 3, were used to provide static pressure taps (three), Kiel

11

probes (17) and Kiel/thermocouple combination probes (three). The placement of these

probes is shown in Table 2.

Probe #	Probe Type	Radial Distance (y)	Angle	
24	Kiel	1.3	15	
27	Kiel	1.6	30	
30	Kiel	1.85	45	
43	Static Port	N/A	60	
13	Kiel	0.2	75	
16	Kiel	0.5	90	
19	Kiel	0.8	105	
22	Combo	1.1	120	
25	Kiel	1.4	135	
28	Kiel	1.7	150	
plug	N/A	N/A	165	
42	Static Port	N/A	180	
14	Kiel	0.3	195	
17	Kiel	0.6	210	
20	Kiel	0.9	225	
23	Combo	1.2	240	
26	Kiel	1.5	255	
29	Kiel	1.8	270	
11	Kiel	0.05	285	
41	Static Port	N/A	300	
12	Kiel	0.1	315	
15	Kiel	0.4	330	
18	Kiel	0.7	345	
21	Kiel	1	360	

Positive Angle

+ y inches

View Looking Downstream

Table 2.   Location of Probes at the Stage Exit After Ref. 2

D.   DATA ACQUISITION SYSTEM

1.   Hardware

A schematic of the data acquisition system is shown in Fig. 7.   The HP75000 Series B VXI-Bus Mainframe was used with an internal digital voltmeter (DVM), a switchbox multiplexer, two scanning multiplexers, a counter, and a Quad 8-bit Digital I/O Module.
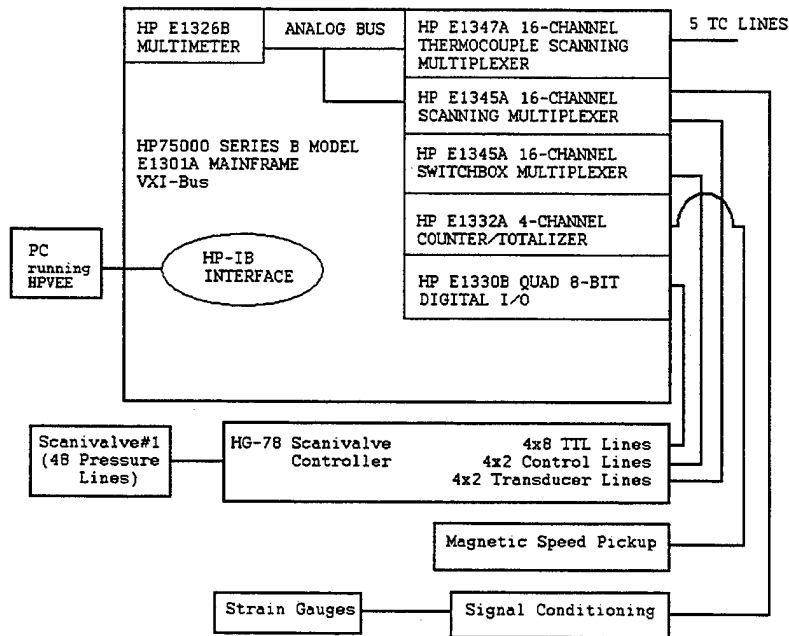
Figure 7.   Schematic of the Data Acquisition System After Ref. 2

An HP-IB (IEEE-488) interface cable facilitated communication between the personal computer and the HP75000 Series B VXI-Bus Mainframe. The cards in the mainframe controlled the Scanivalve operation and digitally acquired pressure transducer measurement, strain gauge measurements, thermocouple measurements, and one frequency measurement (RPM).

a.   *Scanivalve Control*

All pressure lines were connected to a 48-port electrically controlled pneumatic Scanivalve [Ref. 2]. The HP E1345A 16-Channel multiplexer controlled the 'stepping' to each of the 48 ports, and 'homing' to port 1. The port ID was read using the HP E1330B Quad 8-Bit I/O. The Scanivalve transducer was digitized using the HP E1326B multimeter, through the HP E1345A scanning mulitiplexer. Programming was used to select which pressure ports to select, and which ports to skip. The assignment of the 48 Scanivalve ports is shown in Table 3.

Port #	Scanivalve 1
1	Tare
2	Scale
3	Flow Nozzle P6
4	Flow Nozzle Ps
5	Inlet Ptinfinity 1 Q1 4 O'clock
6	Inlet Ptinfinity 2 Q1 8 O'clock
7	Pnozzle static
8	(atmosphere)
9	(atmosphere)
10	(atmosphere)
11	Kiel Probe
12	Kiel Probe
13	Kiel Probe
14	Kiel Probe
15	Kiel Probe
16	Kiel Probe
17	Kiel Probe
18	Kiel Probe
19	Kiel Probe
20	Kiel/TC Combination
21	Kiel/TC Combination
22	Kiel/TC Combination
23	Kiel Probe
24	Kiel Probe
25	Kiel Probe
26	Kiel Probe
27	Kiel Probe
28	Kiel Probe
29	Kiel Probe
30	Kiel Probe
31	Hub Static Pressures P2 1
32	Hub Static Pressures P2 2
33	Hub Static Pressures P2 3
34	Hub Static Pressures P2 4
35	Hub Static Pressures P3 1
36	Hub Static Pressures P3 2
37	Hub Static Pressures P3 3
38	Hub Static Pressures P3 4
39	Shroud Static Pressure P1 3 O'clock
40	Shroud Static Pressure P1 10 O'clock
41	Shroud Static Pressure P3 3 O'clock
42	Shroud Static Pressure P3 6 O'clock
43	Shroud Static Pressure P3 10 O'Clock
44	Shroud Static Pressures Old Style 1 P3
45	Shroud Static Pressures Old Style 2 P2
46	Shroud Static Pressures Old Style 3 P1
47	Shroud Static Pressures Old Style 4 P1
48	Shroud Static Pressures Old Style 5 Pi

Table 3.   Scanivalve Port Assignments After Ref. 2

b.   *Multiplexer Scanning*

Two types of scanning multiplexers were used to collect temperature and strain gauge data from the test rig. The first was a thermocouple multiplexer module (HP E1347A), which was used to acquire the voltages from the thermocouples, and to provide a reference temperature necessary to convert voltages to temperature measurements. The second was a standard relay mulitplexer module (HP E1345A) which, controlled by the digital voltmeter (DVM) driver in the HPVEE program, was used to read the torque-flexure (and Scanivalve) strain gauges.

The thermocouple multiplexer measured the five temperatures directly, as well as measuring the differential voltages between the thermocouple located forward of the rotor (Tinf), and those located aft of the stator (T3). Table 4 shows the connections to the two scanning multiplexers used in the data acquisition process.

Multiplexer Channel	Thermocouples/Mux 100 HP E1347A	DVM Scanner/Mux 200 HP E1345A
00		Scanivalve 1 Transducer
01	Total Temperature Station Infinity @ 4 o'clock	
02	Total Temperature Station Infinity @ 8 o'clock	
03	Total Temperature Station 3 Probe 21	
04	Total Temperature Station 3 Probe 22	Torque -Flexure Strain Gauge Array
05	Total Temperature Station 3 Probe 23	
06		
07		
08		
09		
10		
11	Temperature Differential between channels 1 and 3	
12	Temperature Differential between channels 1 and 5	
13		
14		
15		

Table 4.   Scanning Multiplexer Channel Assignments After Ref. 2

2.   Software

HPVEE software was used to control the instrumentation. The HPVEE software also provided immediate data reduction and conversion to engineering units, allowing real-time feedback on the validity of the data recorded. Reduced and raw data were written to separate data files, for further reduction, plotting and comparison. The HPVEE programs, as well as documentation on the programs, can be found in Appendix D.

E.   DATA REDUCTION

The data were reduced using HPVEE programs (Appendix D). The final form of the data reduction is described below.

The mass flow rate (in lb_m/sec) through the flow nozzle was given by

$$\dot{m} = 16.5424 \cdot C \cdot \sqrt{\frac{P_t \cdot \Delta_s}{459.7 + T_{t_{inf}}}} \cdot \left(1 - 0.039346 \cdot \frac{\Delta_s}{P_t}\right) \tag{1}$$

where $\Delta_s = (P_t - P_s)$ was in inches of water and P_t was in inches of mercury. The constant C represents the flow nozzle coefficient, which was calibrated to be 1.03.

There were two methods of measuring the power absorbed by the compressor. The first measure of horsepower was based on the torque (M) and speed (N) measurements, and was calculated as

$$HP_1 = 1.5865 \times 10^{-5} \cdot M \cdot N \tag{2}$$

wher M is in inch-pounds, and N is in RPM.

The second measure of horsepower was based on a flow rate $\dot{m}$ and stagnation temperature rise across the stage.

$$HP_2 = 1.4137 \cdot \dot{m} \cdot C_p \cdot (T_{t_3} - T_{t_{inf}}) \tag{3}$$

where $C_p = 0.24$ Btu/lb_m ^oR.

Compressor performance was described in terms of referred quantities,

18

$$\dot{m}_{ref} = \dot{m} \frac{\sqrt{\theta}}{\delta}$$

$$N_{ref} = \frac{N}{\sqrt{\theta}}$$

(4)

$$HP_{ref} = \frac{HP}{\delta \cdot \sqrt{\theta}}$$

$$M_{ref} = \frac{M}{\delta}$$

where $\theta = T_{t_{inf}} / T_{ref}$ and $\delta = P_{t_{inf}} / P_{ref}$, and where $T_{ref} = 518.7^0$ R and $P_{ref} = 29.92$ inches of mercury.

The performance evaluation includes the performance of the stator and rotor combination, and is given by the total-to-total (T-T) pressure ratio and efficiency from station 1 to station 3. The honeycomb flow straightener was necessary for torque measurements, but the losses occurring in this section are not included in the compressor performance.

Efficiency was defined as the ratio of the ideal power required in an isentropic compression to the actual power required. The ideal power was given by

$$IHP = 1.4137 \cdot \dot{m} \cdot C_p \cdot T_{t_{inf}} \cdot \left[\left(\frac{P_{t_3}}{P_{t_{inf}}} \right)^{\frac{\gamma-1}{\gamma}} - 1 \right]$$

(5)

19

where γ is the ratio of specific heats.

Three different methods for calculating total-to-total efficiency were used. Method one (η_1) used the temperature rise and total-to-total pressure ratio across the stage:

$$\eta_1 = \frac{IHP}{HP_2} = \frac{T_{t_{inf}}}{T_{t_3} - T_{t_{inf}}} \cdot \left[\left(\frac{P_{t_3}}{P_{t_{inf}}} \right)^{\frac{\gamma-1}{\gamma}} - 1 \right] \tag{6}$$

The second method used a calculation of the inlet stagnation pressure from the inlet static pressure and measured mass flow rate. (Method 1 (η_1) did not involve the mass flow rate.):

$$\eta_2 = \frac{IHP}{HP_2} = \frac{T_{t_{inf}}}{T_{t_3} - T_{t_{inf}}} \cdot \left[\left(\frac{P_{t_3}}{P_{t_{inf}}} \right)^{\frac{\gamma-1}{\gamma}} \cdot 2 \cdot B_{inf} \cdot X_{inf} - 1 \right] \tag{7}$$

where Binf and Xinf were defined by:

$$B_{inf} = \left[\left(\frac{\gamma}{\gamma-1} \right) \cdot \frac{P_{inf}}{V_t \cdot \left(\dfrac{\overset{\bullet}{m}}{A_{inf}} \right)} \right] \tag{8}$$

20

and

$$X_{inf} = \sqrt{B_{inf}^2 + 1} - B_{inf} \qquad (9)$$

P_{inf} is the wall (static) pressure where the area is A_{inf}, and $V_t = \sqrt{2 \cdot C_p \cdot T_{t_{inf}}}$.

The third method for the calculation of the efficiency (η_3) depended on torque

and mass flow rate, but not on the measurement of temperature rise across the stage.

$$\eta_3 = \frac{IHP}{HP_1} \qquad (10)$$

THIS PAGE INTENTIONALLY LEFT BLANK

III. TEST PROCEDURES AND PROGRAM OF TESTS

A. PROCEDURES

Test preparation consisted of bringing the Allis-Chalmers compressor to a stable speed, providing compressed air to the balance piston, air regulator, and setting the drop rate for the oil-mist bearing lubrication system. The drop rate for the bearing lubrication system was set at 2-3 drops per minute, and was allowed to operate for at least fifteen minutes before testing was initiated. The data acquisition system was checked out and the Scanivalve pressure transducer was calibrated prior to each test.

A typical test was conducted at a constant speed. The run began with the compressor throttle wide open. Data were then taken at various throttle positions, corresponding to desired flow rate changes. When stall occurred, the throttle was opened slightly to stabilize the compressor, and then closed again to closely approach the stall condition. Data were recorded and then the throttle was incrementally opened recording data at each setting, until the throttle again reached the wide open position.

B. PROGRAM OF TESTS

Seven separate test runs were conducted with the Sanger stage in the TCR. The first run was a 50 minute run, without the casewall and intake system attached to the rig, in order to verify the new instrumentation, verify the operation of the oil-mist bearing lubrication system, and the operating instrumentation.

The casewall was installed for the second run, which was intended to achieve 40% design speed At approximately 10,000 RPM, rubbing occurred (visible on the video monitor) between the rotor blades and the casewall. The TCR was immediately shut down. When it was realized that the casewall might have shrunk as a result of cool incoming air temperatures, ice was applied to measure the effect of temperature on the clearance. The ice was sufficient to eliminate tip clearance altogether.

Therefore, before testing was continued, four 'dry heat' heating pads (sold in drugstores for home use) were applied to the casewall, as shown in Fig. 8. Two contact thermocouples (Omega # SA1-J) were set into unused pressure ports in the casewall between the rotor and the stator. The heating pads were then used to, in effect, control the tip clearance of the rotor blades. The heating pads were used in all the remaining runs, with the exception of the varying use of the heating pads noted in the final run.

The third run was conducted without the air intake system connected to the rotor. The purpose of this test was to provide immediate access to the rotor after shutdown, in order to measure tip clearance with the heating pads on. Large clearances were measured because the compressor ingested the air exhausting from the drive turbine, resulting in inlet air temperatures over 80 °F. The inlet pipe was reconnected in order to conduct performance tests with adequate clearances maintained by casewall heating.

The fourth test was conducted at 50% (13,543 RPM) of the design speed (27,085 RPM). Twelve data points were taken, six approaching stall with decreasing mass flow

24
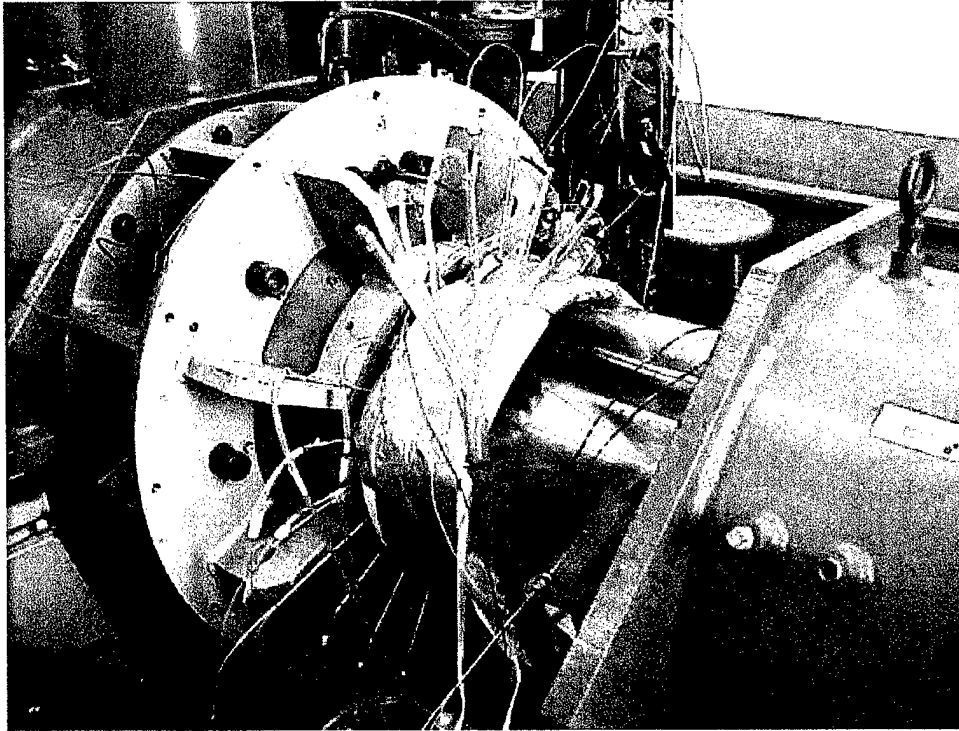
Figure 8.   Casewall with Heating Pads

rate, and six leaving stall with increasing mass flow rate.   The fifth run was conducted at

60% of the design speed (16,200 RPM), with the same number of data points.   The sixth

run was conducted at 70% of design speed (18,960 RPM), with four data points taken

approaching stall, and five data points taken moving away from stall at an increased mass

flow rate.   Stall was encountered (intermittently) at two throttle positions, possibly as a

result of tip clearance varying due to temperature changes in the casewall.

The final run was also conducted at 70% of the design speed, multiple scans were

taken of data at each setting to exam data uncertainty, and an attempt was made to reduce

the tip clearance. Starting with the throttle fully open, the heating pads were left on while

the compressor was throttled from full open to stall.   At each of four flow rate settings,

three data points were taken. Once the compressor reached stall, the heaters were turned off and, after waiting for the casewall to cool, another set of three data points were recorded. Since little change occurred in the casewall temperature the throttle was opened fully, to pump cool air through the casewall. When the casewall had cooled to 95° F, the throttle was closed, to return to the flow rate to that which was set prior to turning off the heaters. The throttle was then opened progressively, taking data with the heaters off. Three sets of three data points were recorded between stall and the full open throttle position.

C.   CASEWALL AND CLEARANCE CHANGES

The casewall was initially installed and the ('cold') tip clearances shown in Fig. 9a were measured using a feeler gauge. Following the contact between the rotor and the casewall during the second test run, the tip clearances shown in Fig 9b were measured. The differences were relatively small, and in the absence of the strong temperature effects on the dimensions of acrylic, a blade rub would not have occurred.

The casewall was manufactured to be within design specifications, at 70-75°F. The temperature of the test cell was kept near 75°F with wall-mounted heaters. However, the coefficient of linear expansion for acrylic is at least 35×10^{-6} ins/in °F [Ref. 5] resulting in at least 0.2 thousandths of an inch change in radius (or clearance) per degree. The growth in aluminum is one third that for Plexiglas. The temperature of the ambient air flowing through the compressor in the initial tests was approximately 60°F, which
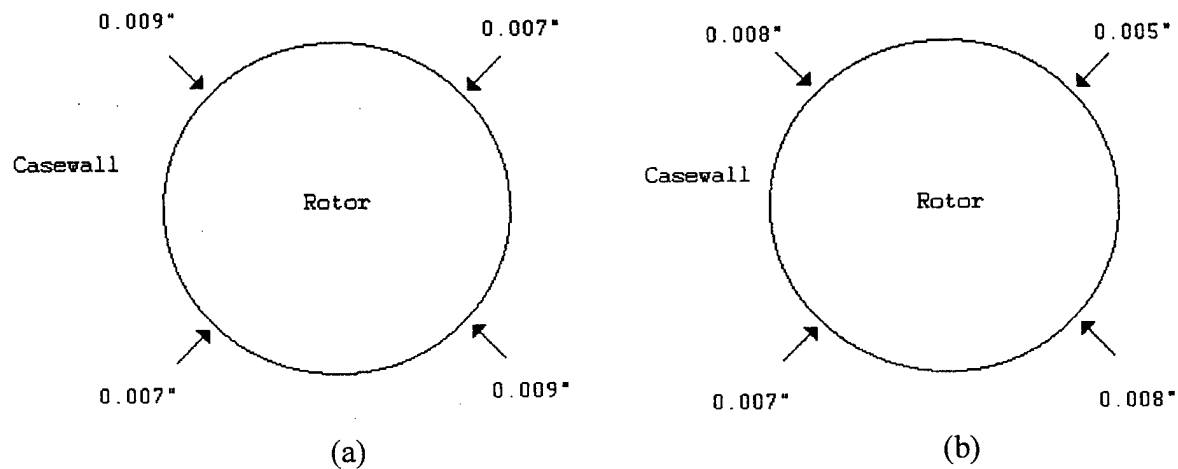
Figure 9. Tip Clearance between Rotor and Casewall Before (a) and After (b)
Contact

would have closed the initial clearance by at least 0.003 inches. After cooling the casewall with ice, and observing that the 0.008" gap could be closed by the effect of the temperature change, it was determined that the casewall had to be heated to prevent further contact with the rotor.

Two thermocouples were embedded in the casewall between the rotor and the stator, and the four heating pads were set on 'medium'. The tip clearance was measured as a function of casewall temperature (as it gradually heated up) under static conditions.

As the casewall temperature increased, the tip clearance between the rotor and the casewall increased as shown in Fig. 10. Since there was an uncertainty in measuring the rotor-casewall tip clearance, a linear approximation of the gap growth as a function of temperature was assumed for the purposes of estimating the running clearance. The casewall temperature was monitored during subsequent testing. Two thermocouple output

27

meters were positioned near the casewall in the test cell and included in the video image observed on the monitor in the control room.

After testing was completed, the tip clearance was measured again, and it was found that it had not changed from the previous measurement of tip clearance that was taken during ambient conditions (Fig. 9b). However, additional contact between the rotor and the casewall had occurred at some point during the previous four test runs. The heating pads obscured the view of the rotor blade tips during testing. Pictures of the initial (after run 2) and subsequent (after run 7) contact between the rotor and casewall are shown in Fig. 11.
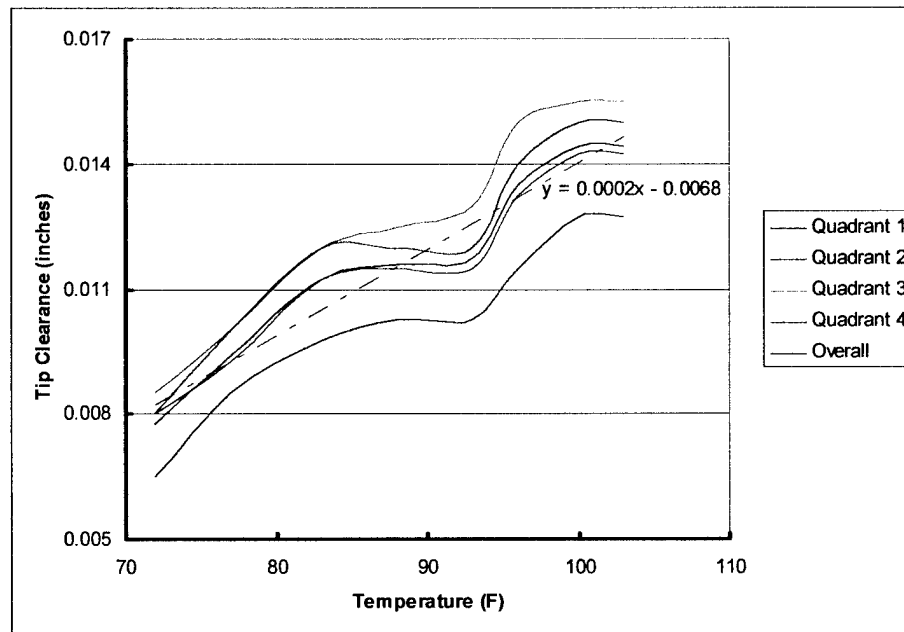
Figure 10.   Casewall Temperature Effect on Static Tip Clearance

From the calibration of the effect of casewall temperature on tip clearance (Fig. 10), and the effect of rotation and temperature on rotor blade extension, the tip clearance

28

expected to be present during each of the test conditions was calculated. The results are shown in Fig. 12. While significant clearances were calculated, contact had occurred during at least one of the last four runs. Therefore, until the effect of wall heating on tip clearance could be monitored by measurements during operation, no attempt was made to increase the operating speed.

(a)

(b)

Figure 11.   Casewall After Initial (a) and Subsequent (b) Contact
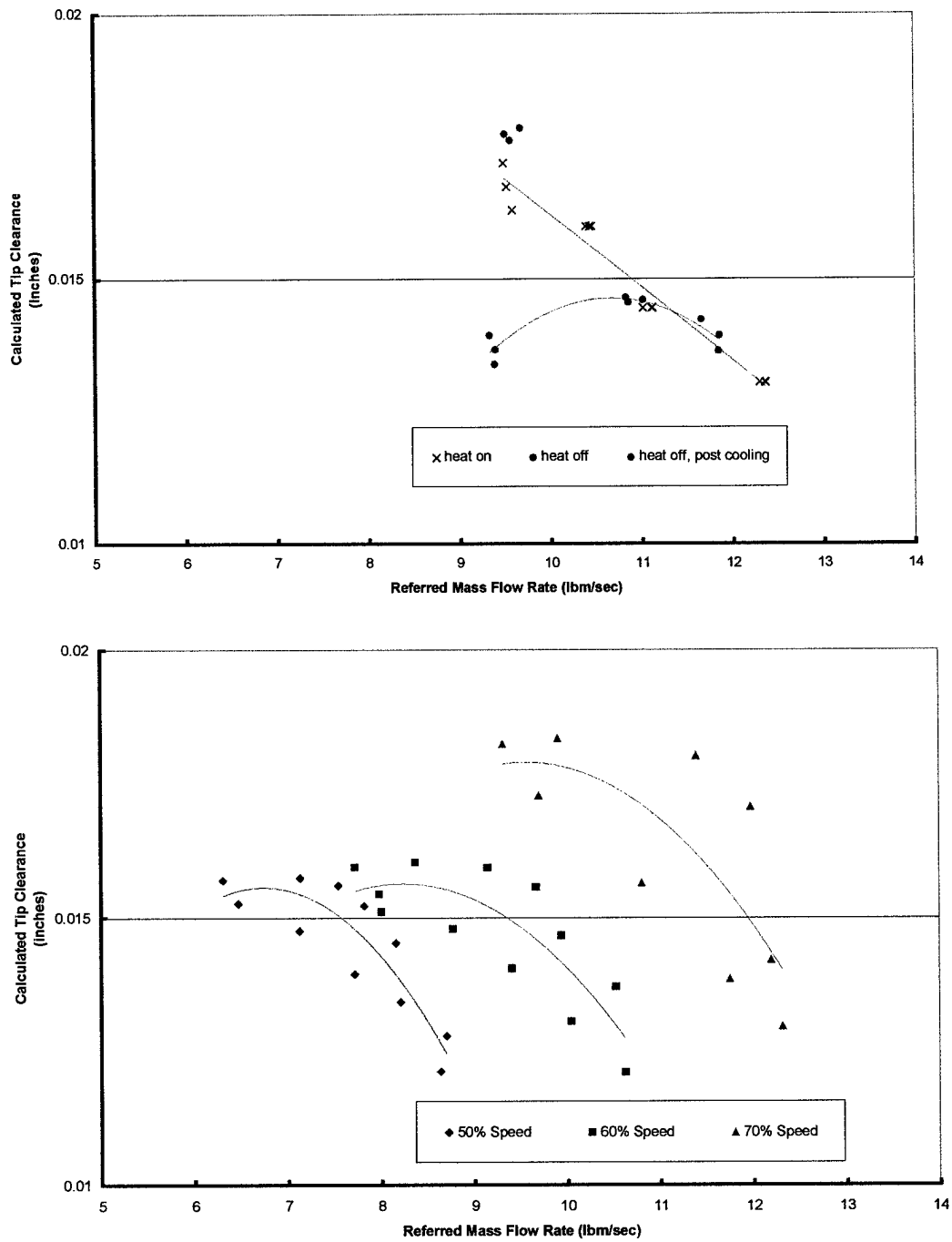
Figure 12.   Calculated Tip Clearance for Test Conditions

THIS PAGE INTENTIONALLY LEFT BLANK

IV. RESULTS AND DISCUSSION

A. INTRODUCTION

The performance of the Sanger Stage was measured at 50%, 60% and 70% of the design speed of 27,085 rpm. No changes were made to the instrumentation, data acquisition or reduction procedures, with the exception of varying the trigger level on the counter/totalizer in the HPVEE speed pickup program, throughout the series of tests, Each of the plotted experimental data sets was fitted with a second order polynomial. A complete reduced data listing is included in Appendix C.

B. STAGE PERFORMANCE

The total-to-total pressure ratio (Fig. 13-15) , adiabatic efficiency (Fig. 16-21), referred torque (Fig. 22 and 23), stage temperature rise (Fig. 24 and 25) and referred horsepower (Fig. 26 and 27), were plotted as a function of the referred mass flow rate, for constant speed conditions. The speed condition is expressed as a percentage of the design speed (27,085 rpm). Comparison with stage performance predictions using the multi-blade-row SWIFT code [Ref. 6], and previous experimental work conducted by Grossman [Ref. 2], are shown for 70% and 80% of the rotor design speed.

Figure 13 shows the measured total-to-total pressure ratio vs. referred mass flow rate at 50%, 60% and 70% speed and the results of predictions using the SWIFT code. The code prediction at 70% speed follows closely the trends in the experimental results.

It is noted that the tip clearance in the experiment (0.013 – 0.017 inches) was calculated to be larger than the design value assumed in the computation (0.004 inches). This would be consistent with a lower pressure ratio measured in the experiment. Figure 14 shows a comparison between experimental results conducted after the rebuild of the TCR, and work conducted by Grossman [Ref. 2] with the initial build of the Sanger stage. Reasonable agreement is observed near open throttle and some departure closer to stall. Figure 15 shows that the pressure ratio increase with decrease in flow rate, was greater when the casewall was cooled. Thus the difference between the present and Grossman's results could be due to differences in clearance.

Three different efficiency plots were produced, based on the efficiencies defined in equations (6), (7) and (10). The efficiency η_3 was expected to be the most accurate, because it used both torque and speed measurements to provide a proper integral measurement of compressor work. It was apparent however that there was an unexpected uncertainty in the torque measurement and therefore in the value calculated for η_3. Both efficiency η_1 and efficiency η_2 used the temperature rise across the compressor stage. While the compressor inlet temperature can be expected to be uniform across the inlet flow, temperature measurements were taken at only three locations in the flow behind the stator (Table 2), and a radial temperature profile would be expected there..

Figures 16, 17 and 18 show the adiabatic efficiencies (η_1, η_2 and η_3 respectively) calculated for the 50%, 60% and initial 70% test runs. Figure 16 also shows the efficiency computed using the SWIFT code. Clearly, the magnitudes of η_1 and η_2 are

too large, since they either approach or exceed unity at the peaks. Since the stagnation pressure rise is computed from a representative map of the exit flow field, and the temperature rise from just three probe measurements, the error is most probably in the magnitude of the temperature rise. Unfortunately, the efficiency that does not require temperature rise measurements, η_3, was not well-behaved. This efficiency used torque and speed, and the torque measurement was observed to change to a more credible level when the compressor was first stalled at 50%. Figure 18 shows however that subsequent points were not well behaved. Figures 19, 20 and 21 show the adiabatic efficiencies calculated from the tests conducted at 70% while varying the heating of the casewall. All three efficiency calculations in Figs. 19, 20 and 21, show that efficiency decreased when the casewall was cooled. This was not to be expected since the pressure ratio increased when the casewall was cooled (Fig. 15).

Figures 22 and 23 show the effect of flow rate on torque required, for the three speeds and for the second test conducted at 70% respectively. At the lower two speeds in Fig. 22, there is observed to be a hysteresis in the torque behavior between throttle closing (lower), and throttle opening (higher), which would be consistent with friction in the system. None was detected when the stator movement was checked after the tests. Uncertainty in the torque measurements, indicated by the scatter observed in the torque readings, was greater than to be expected from the calibration (Appendix B). (Re-calibration was postponed since it required the removal of the casewall and rotor assemblies).

Figures 24 and 25 show the behavior of the stage temperature rise as the compressor was throttled. The stage temperature rise was calculated using the average of the differential temperatures between one probe located upstream of the rotor, and two probes located downstream of the stator. It is noted that the uncertainty (that indicated only by the scatter) in the data in Fig. 24, increased with compressor speed (and magnitude of temperature rise), suggesting the need to examine the sampled data.

Figures 26 and 27 show a comparison of the horsepower required by the compressor stage, calculated using the two different methods. The horsepower calculated using the temperature rise across the stage has less uncertainty (based on the observed scatter) than that calculated using the torque and speed measurements. The 50% speed line in Figs. 22 and 26 shows the effect of the significant increase in torque that was measured immediately following the first compressor stall. It is noted that following this event, the measures of horsepower were in reasonable agreement at open throttle. Near to stall, horsepower based on temperature rise exceeded that based on torque. This is likely to be the result of changes in the outlet temperature distribution, which is not properly averaged by only three fixed temperature probes.

C.   PRESSURE PROFILES

The variations in the stage total pressure ratio as a function of radial distance from the inner wall of the casing are shown for the 50%, 60% and 70% design speed performance tests in Figs. 28, 29 and 30 respectively. Three different referred mass flow

rates are shown at each speed. The Sanger stage was designed to have nearly uniform total pressure distribution across the exit [Ref. 1]. The plots show that with the exception of the pressure probe (24) located 1.3 inches radially from the casewall, the total pressure distribution was nearly uniform across the exit.
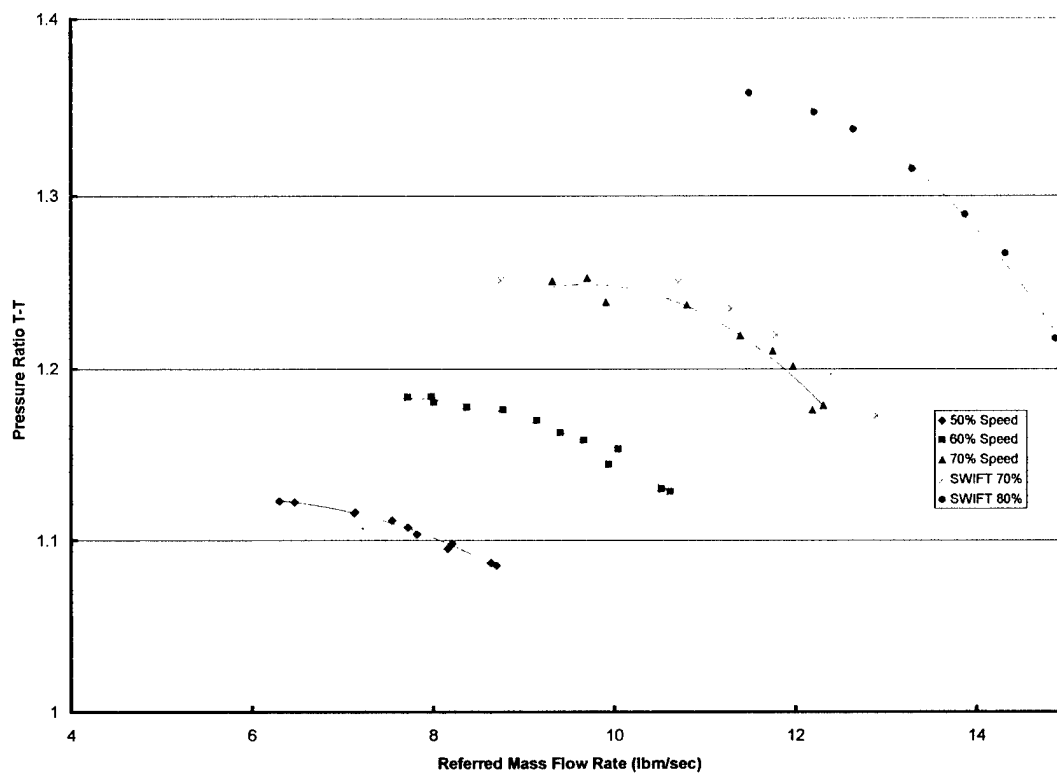
Figure 13.   Stage Pressure Ratio (T-T) vs. Referred Mass Flow Rate
Comparison of Test Results with CFD Predictions
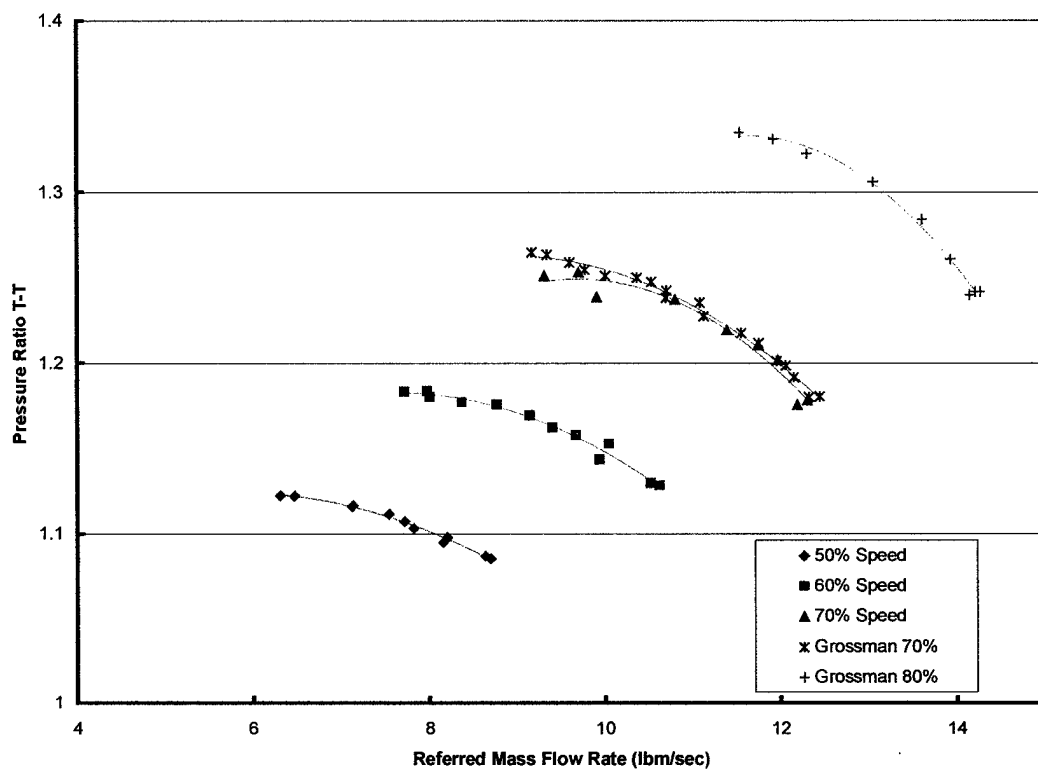
Figure 14.   Stage Pressure Ratio (T-T) vs. Referred Mass Flow Rate
Comparison of Present and Earlier Test Results
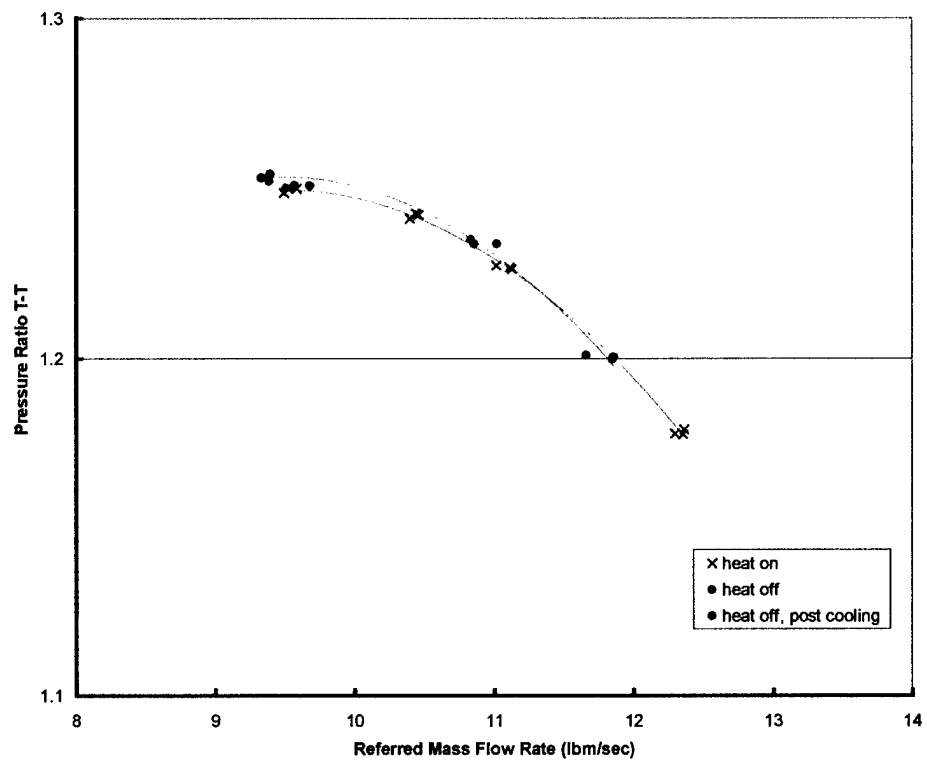
Figure 15.   Stage Pressure Ratio (T-T) vs. Referred Mass Flow Rate, Effect of
Casewall Temperature
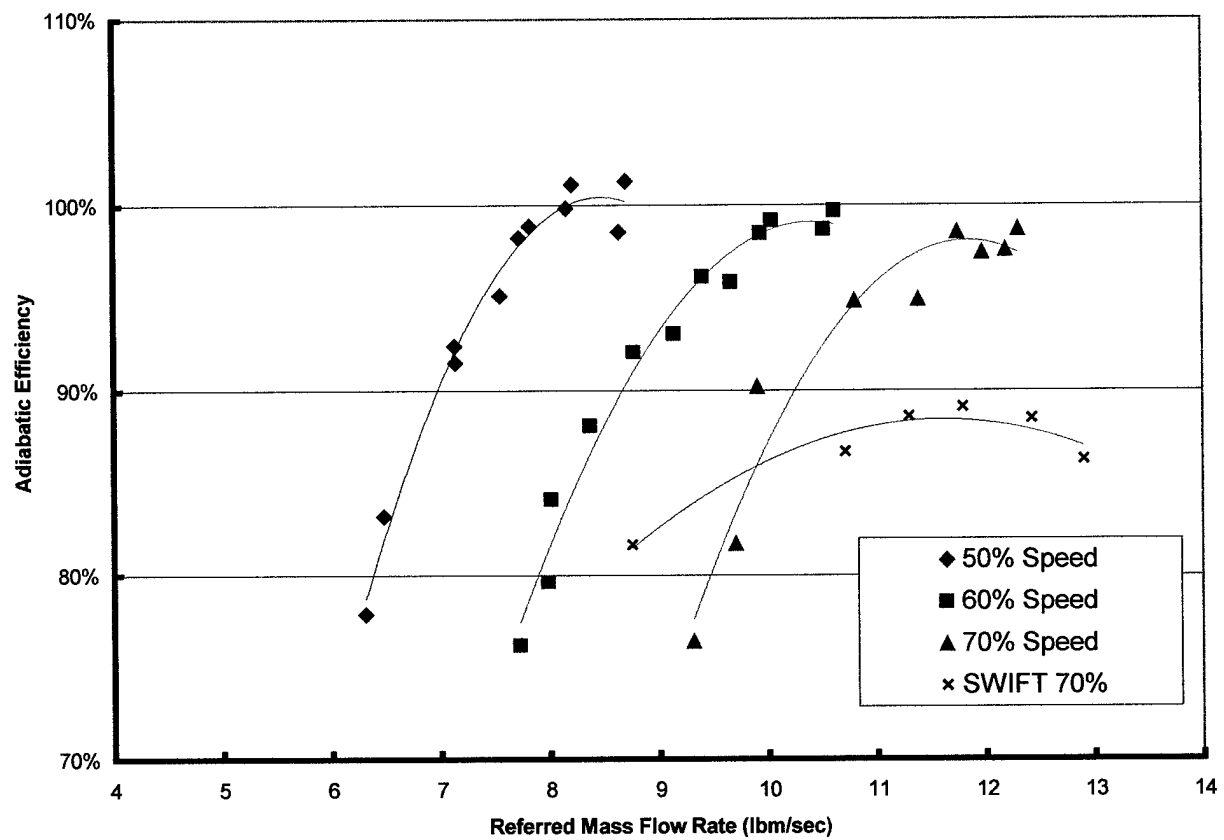
Figure 16.   Adiabatic Efficiency (η_1) vs. Referred Mass Flow Rate
Comparison of Test Results with CFD Predictions
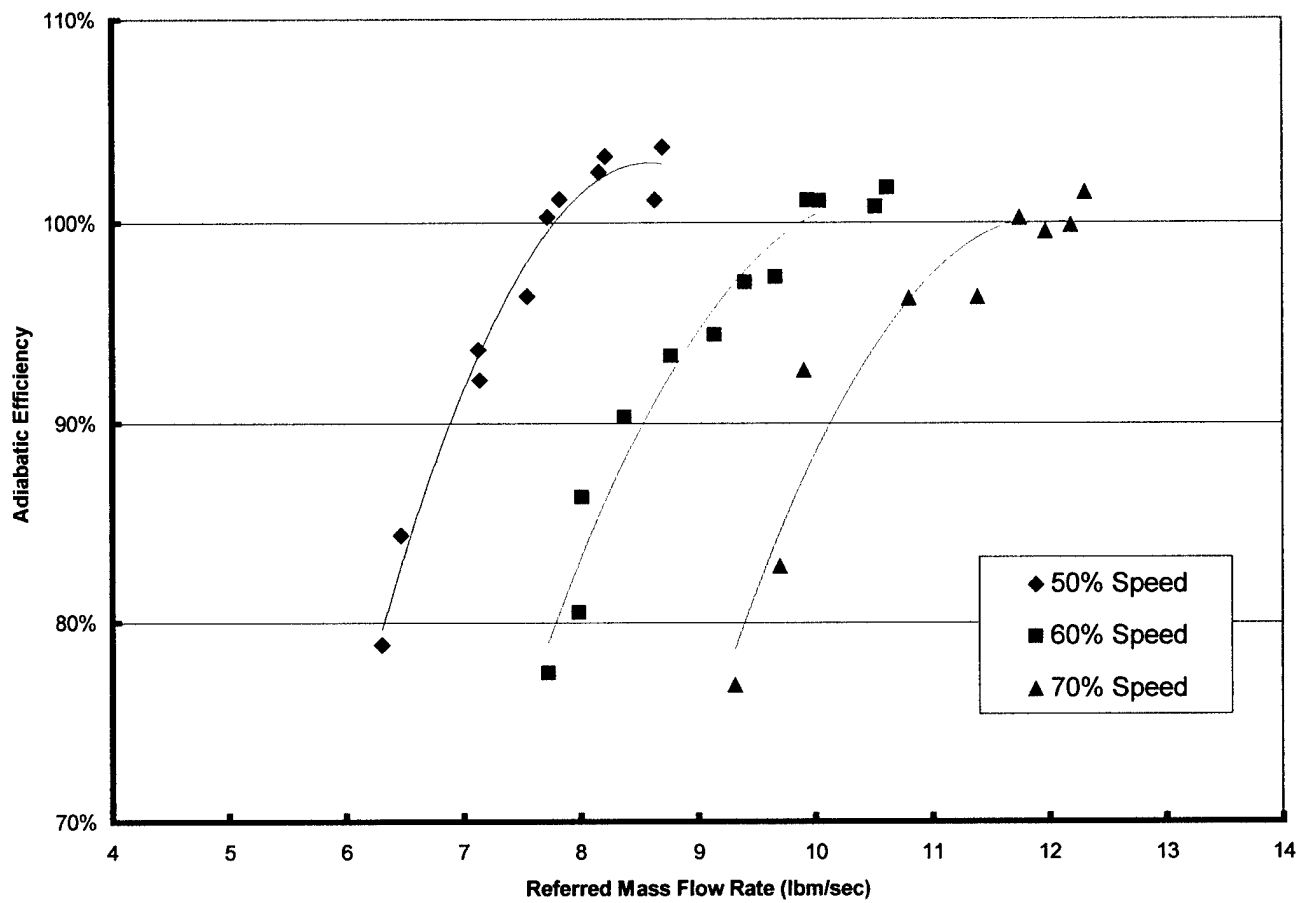
Figure 17.   Adiabatic Efficiency (η_2) vs. Referred Mass Flow Rate
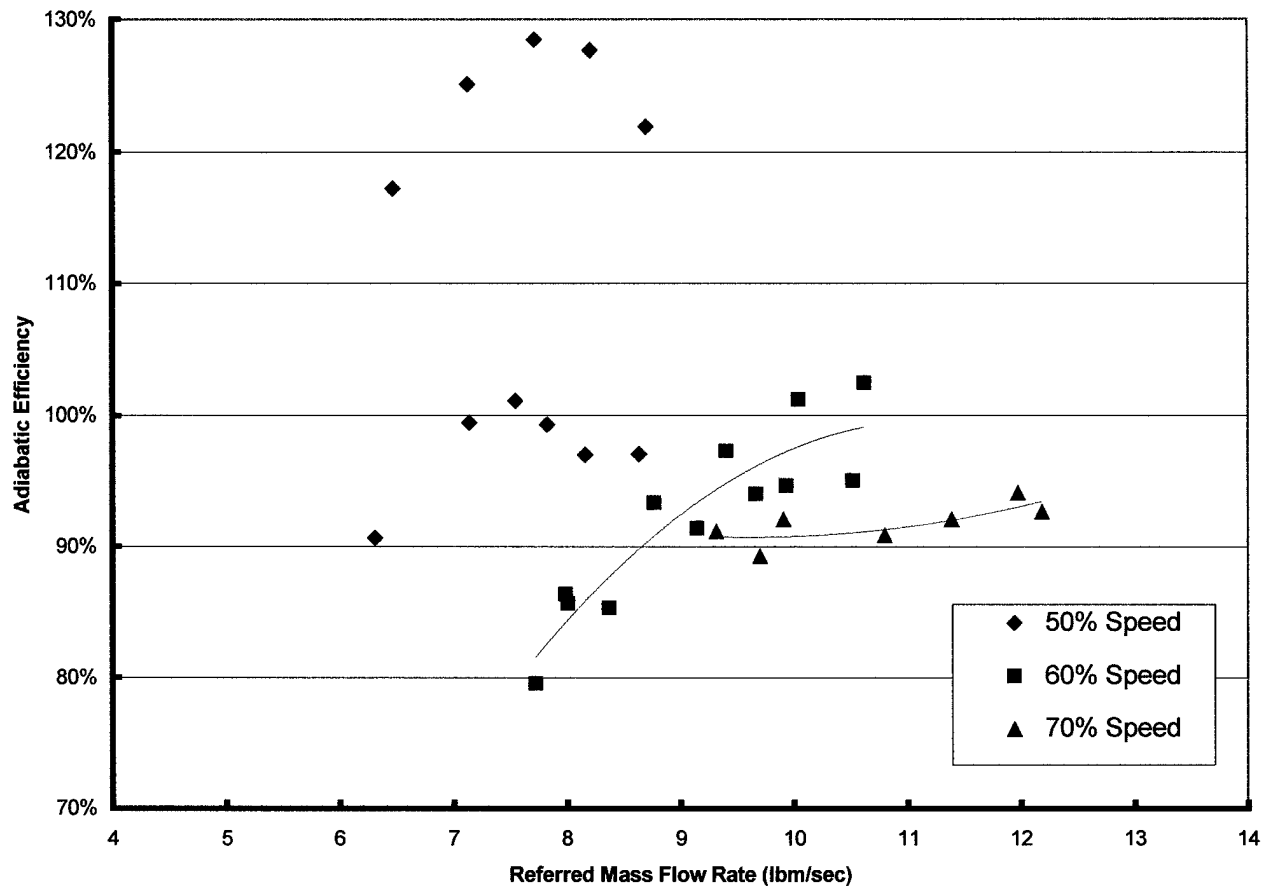
Figure 18.   Adiabatic Efficiency (η_3) vs. Referred Mass Flow Rate
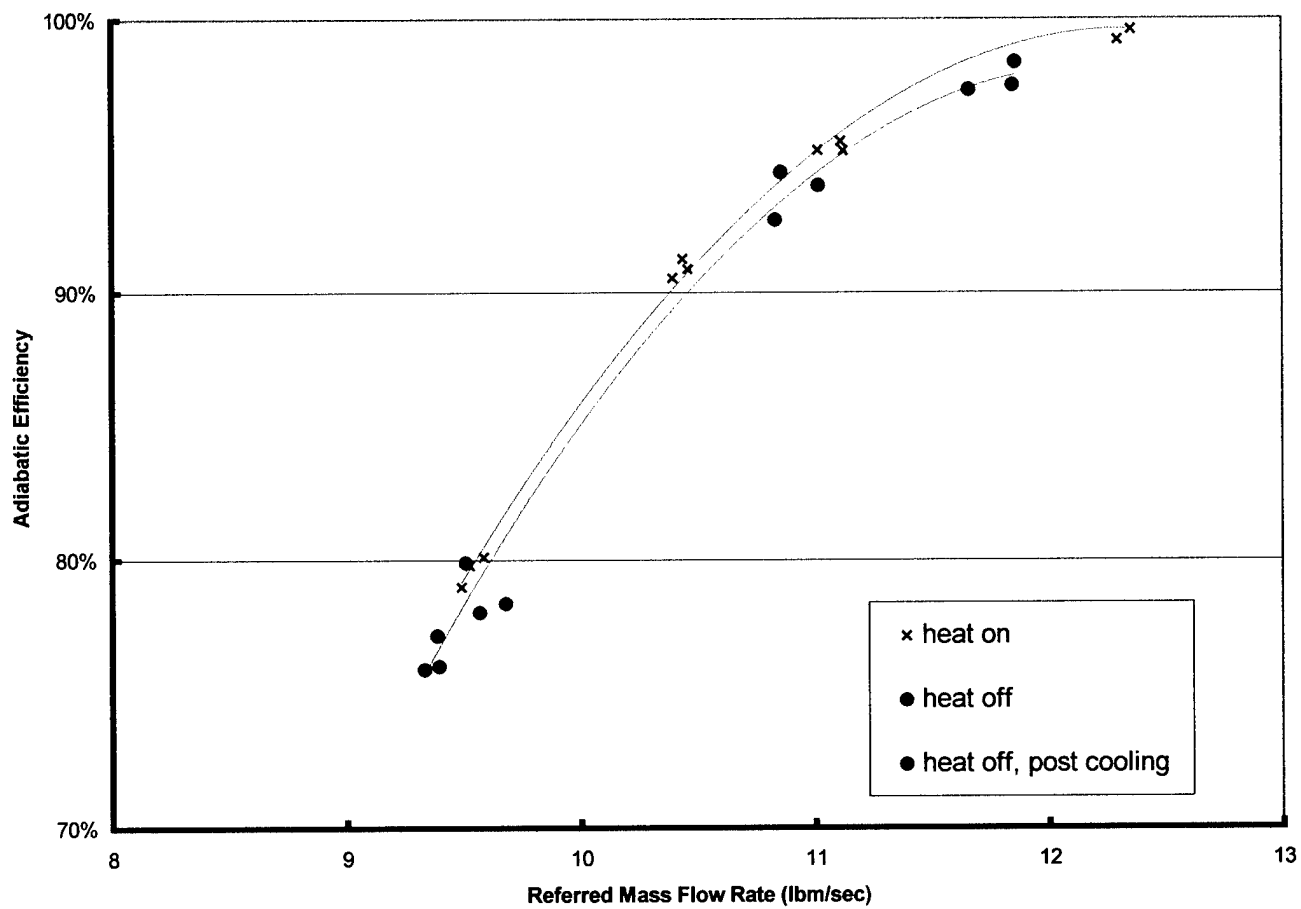
Figure 19.   Adiabatic Efficiency (η_1) vs. Referred Mass Flow Rate Effect of
Casewall Temperature
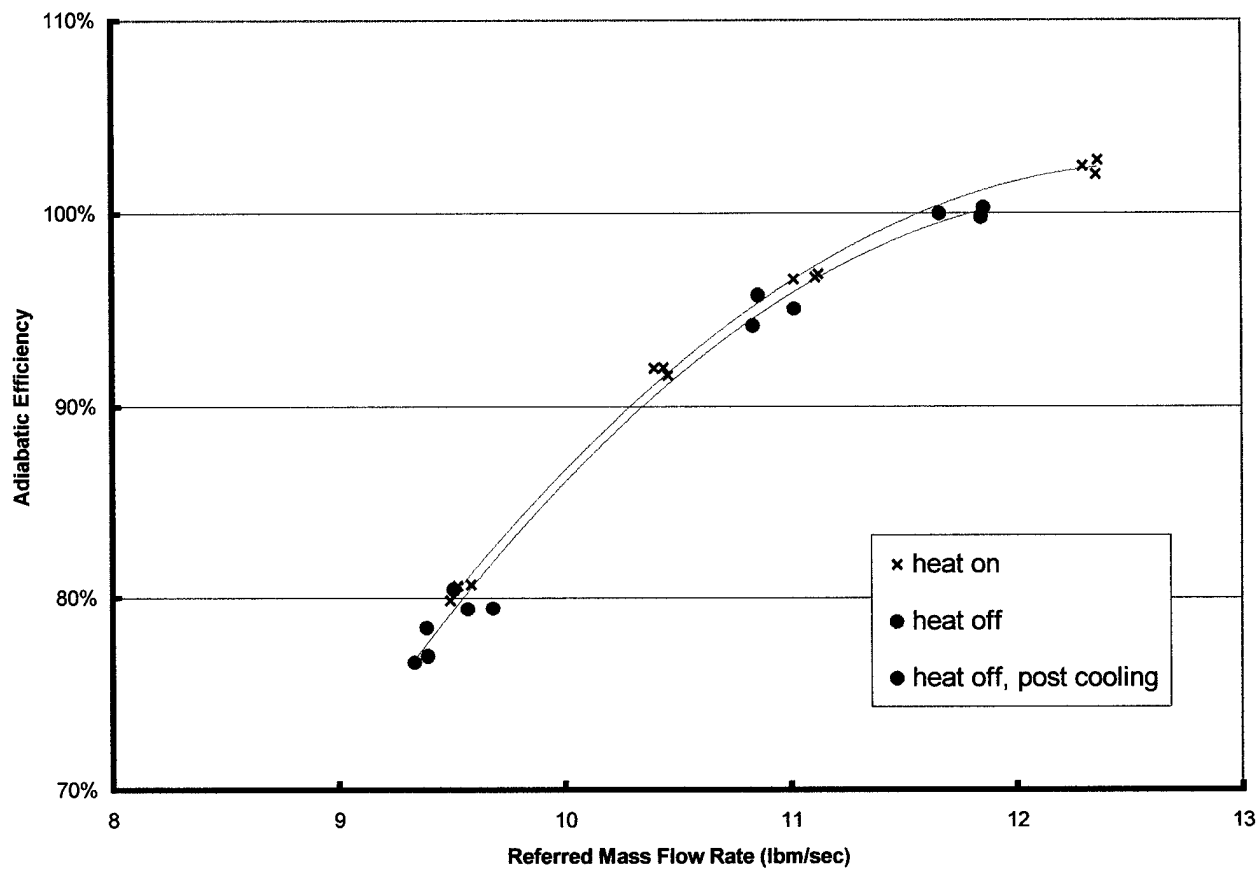
Figure 20.   Adiabatic Efficiency (η_2) vs. Referred Mass Flow Rate Effect of
Casewall Temperature

Figure 21.   Adiabatic Efficiency (η_3) vs. Referred Mass Flow Rate Effect of
Casewall Temperature
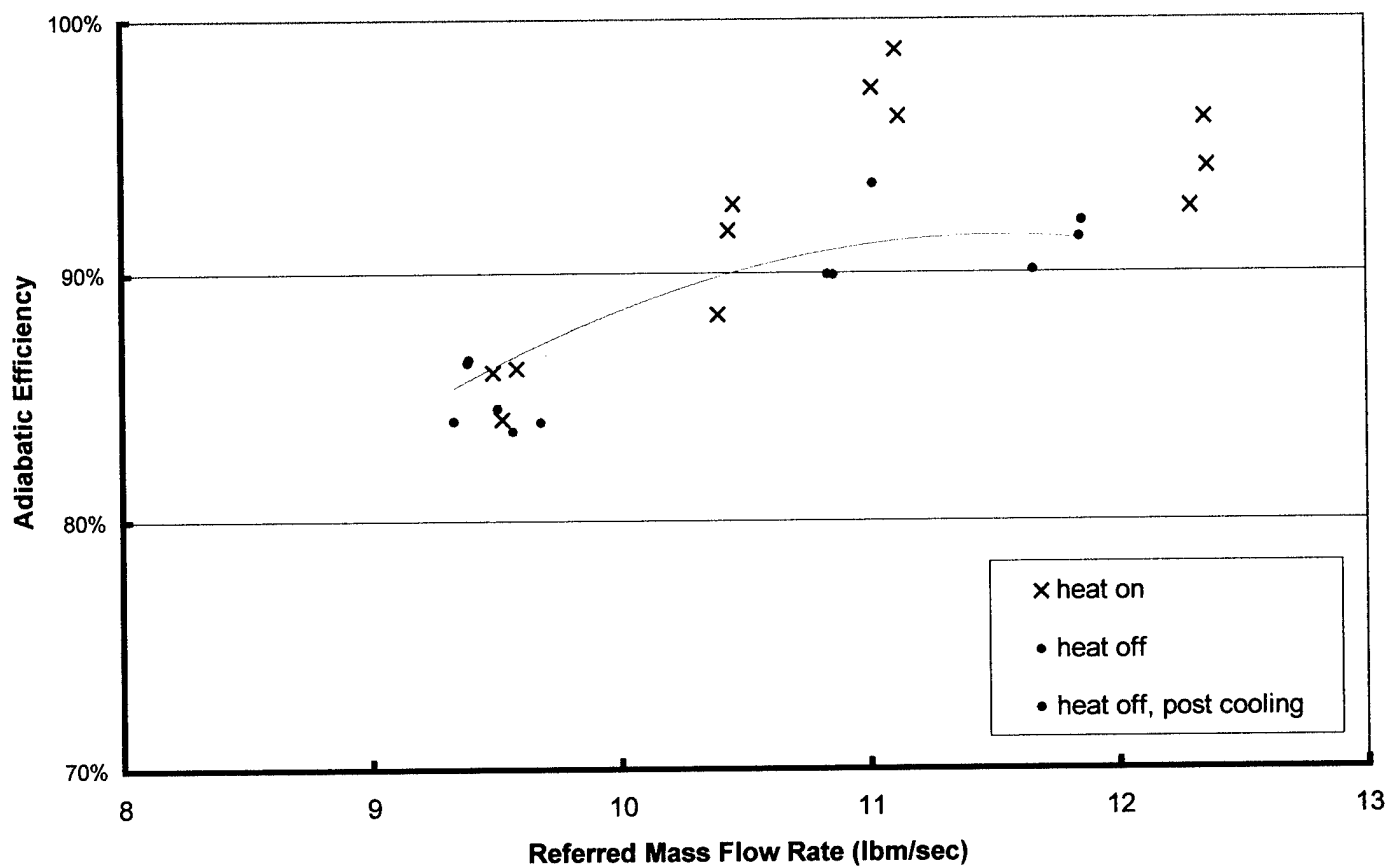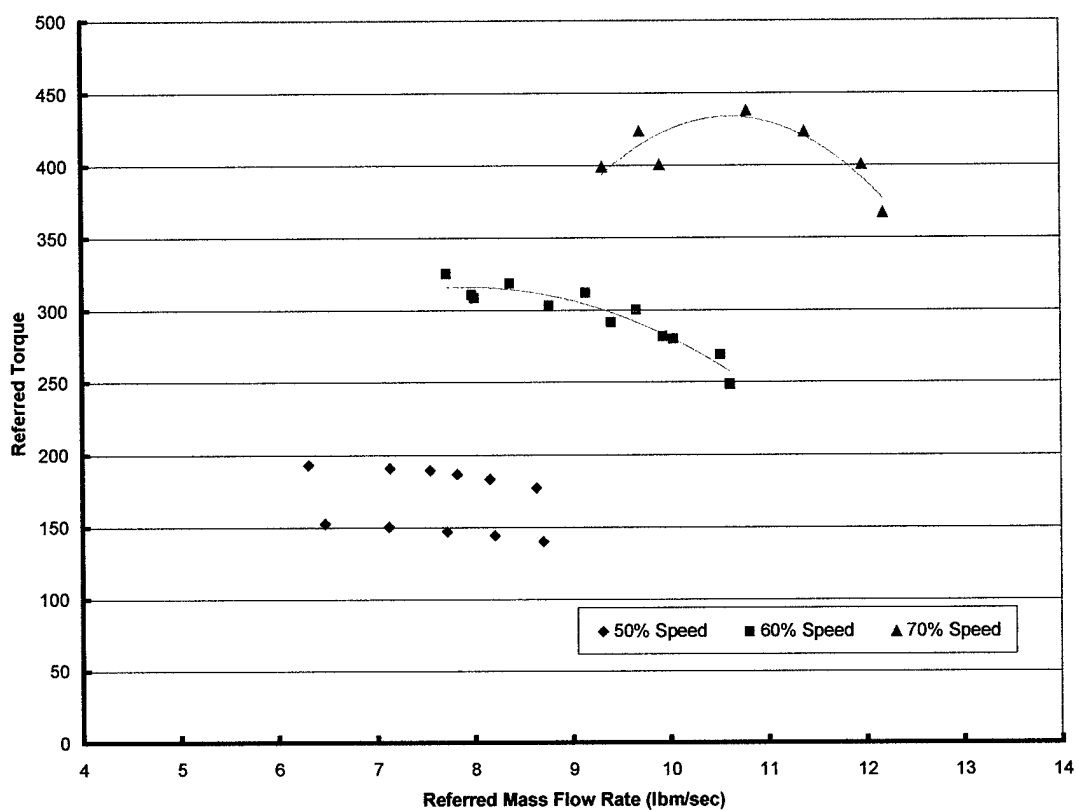
Figure 22.   Referred Torque vs. Referred Mass Flow Rate
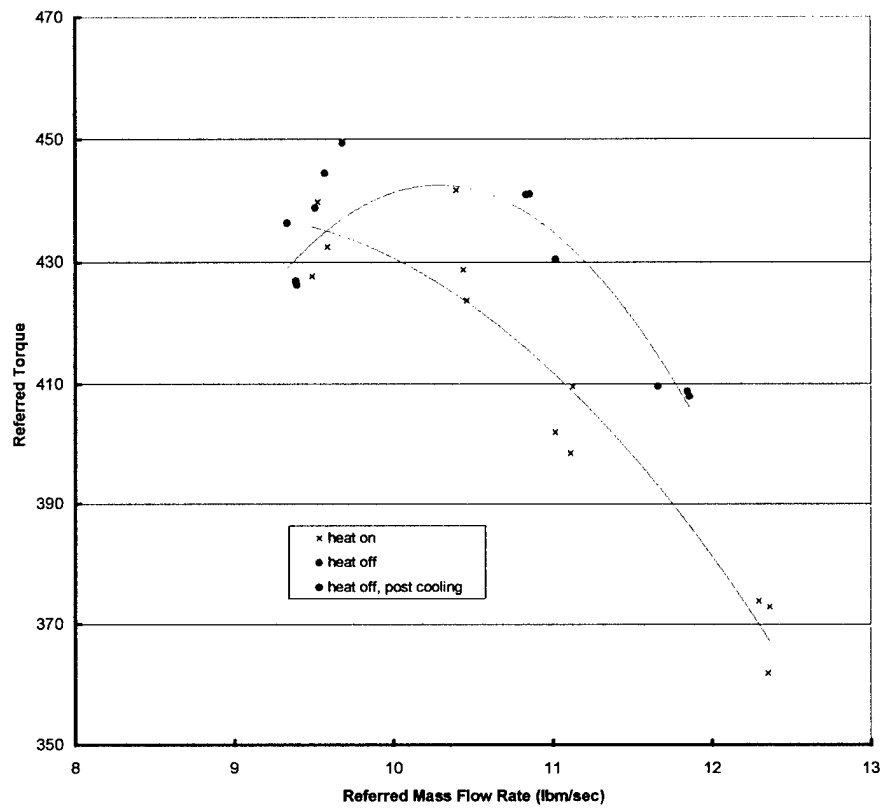
Figure 23.   Referred Torque vs. Referred Mass Flow Rate (Temperature
Effect)
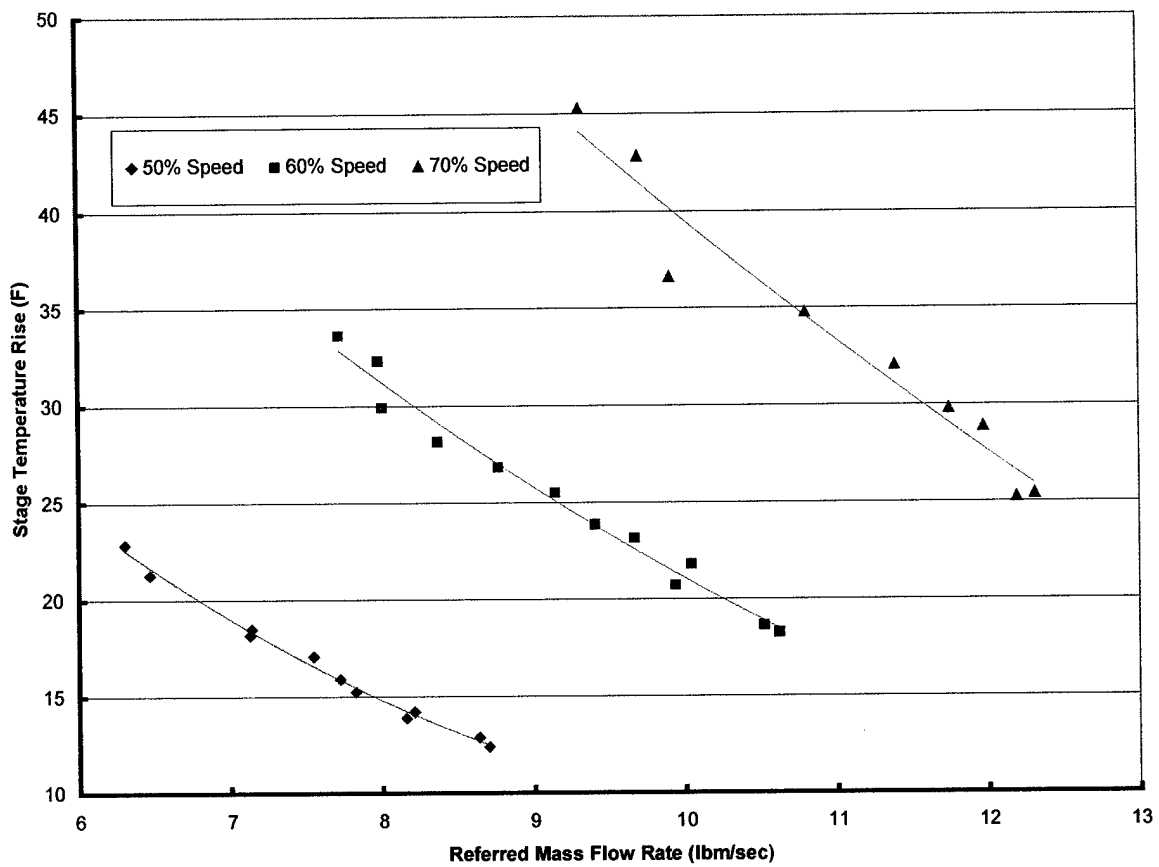
Figure 24.   Stage Temperature Rise vs. Referred Mass Flow Rate
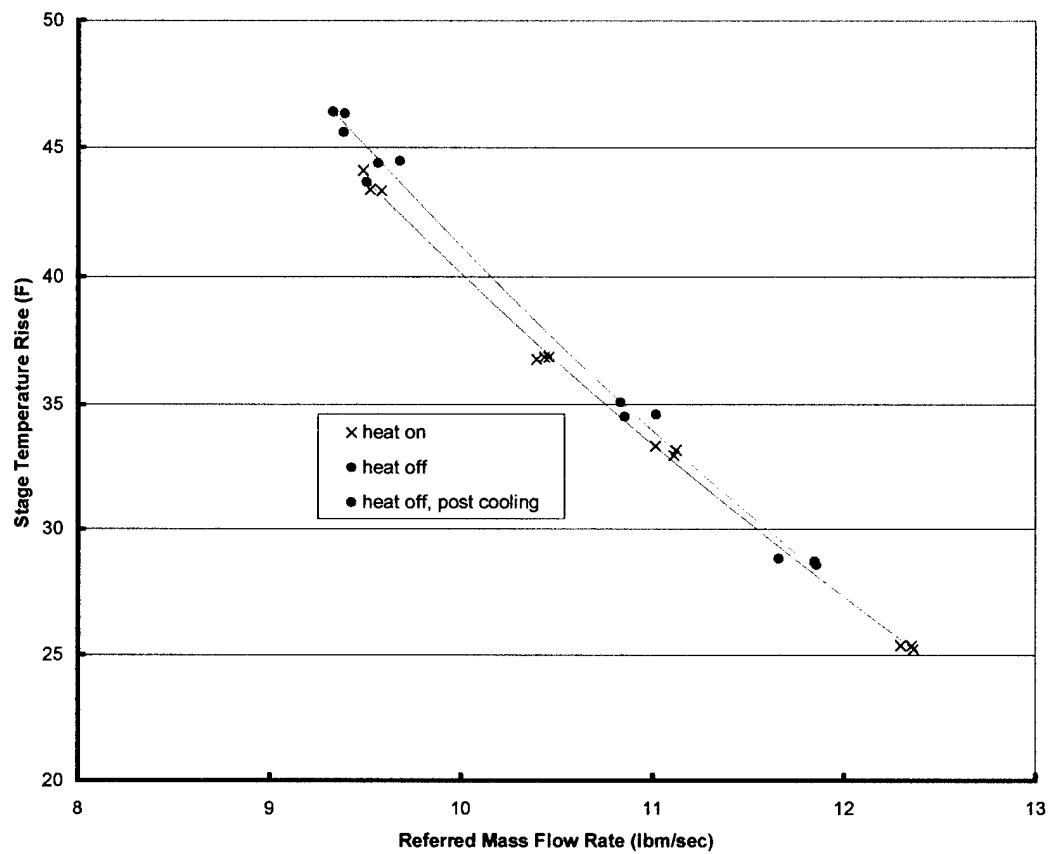
Figure 25.   Stage Temperature Rise vs. Referred Mass Flow Rate Effect of
Casewall Temperature
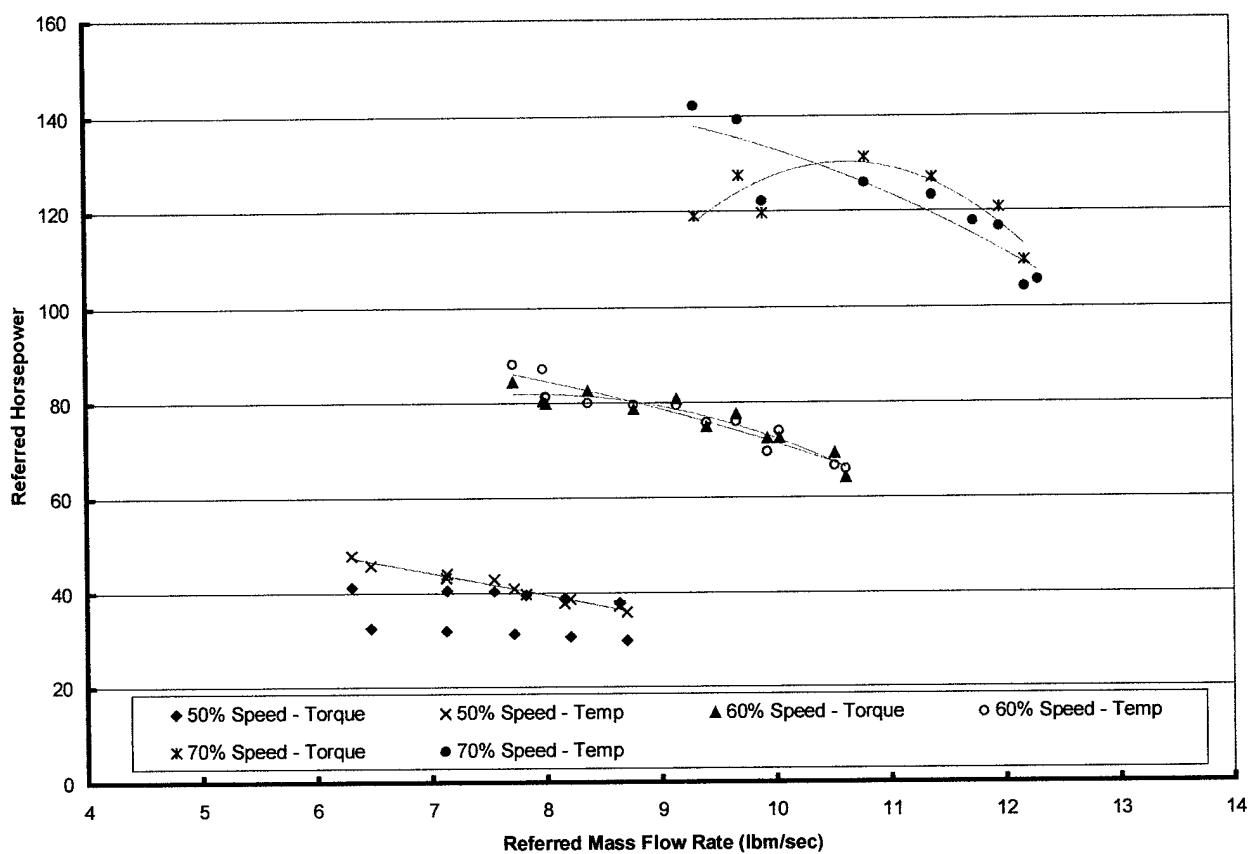
Figure 26.   Referred Horsepower vs. Referred Mass Flow Rate
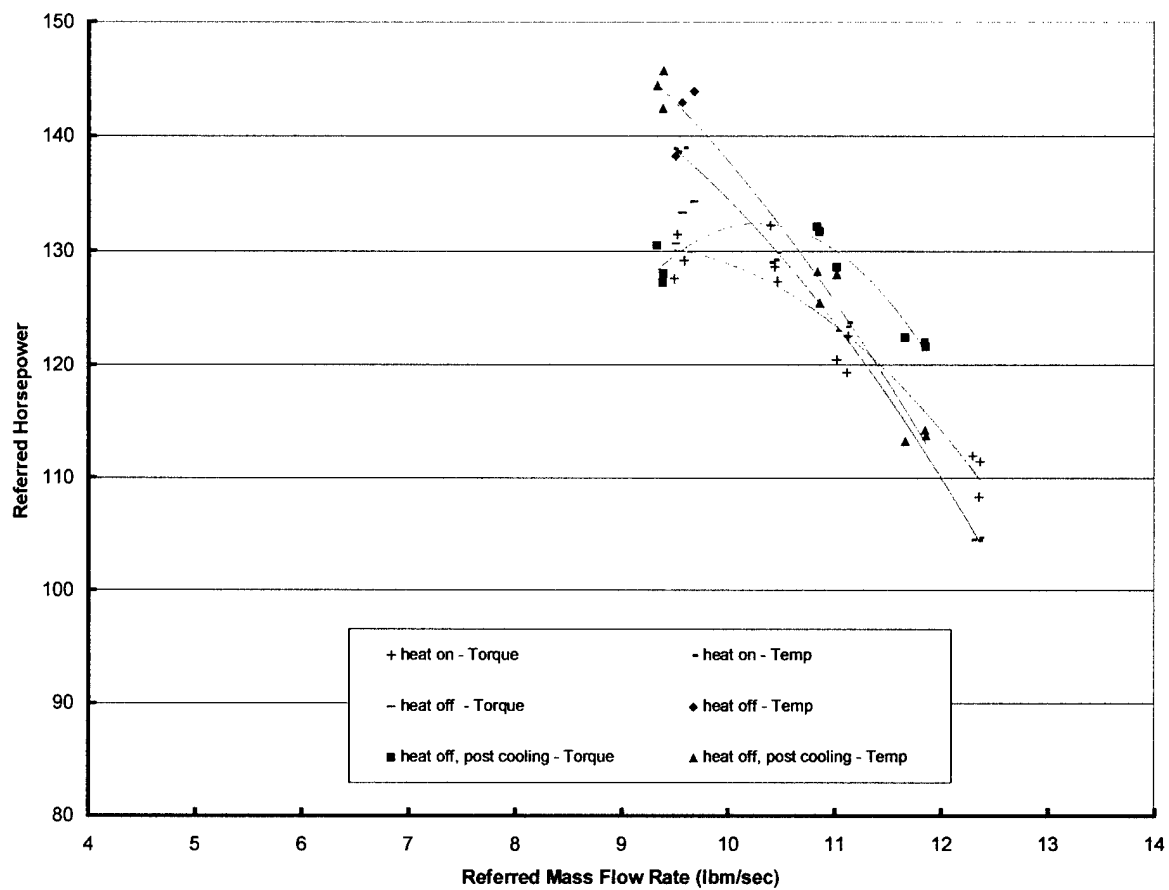
Figure 27.   Referred Horsepower vs. Referred Mass Flow Rate Effect of
Casewall Temperature
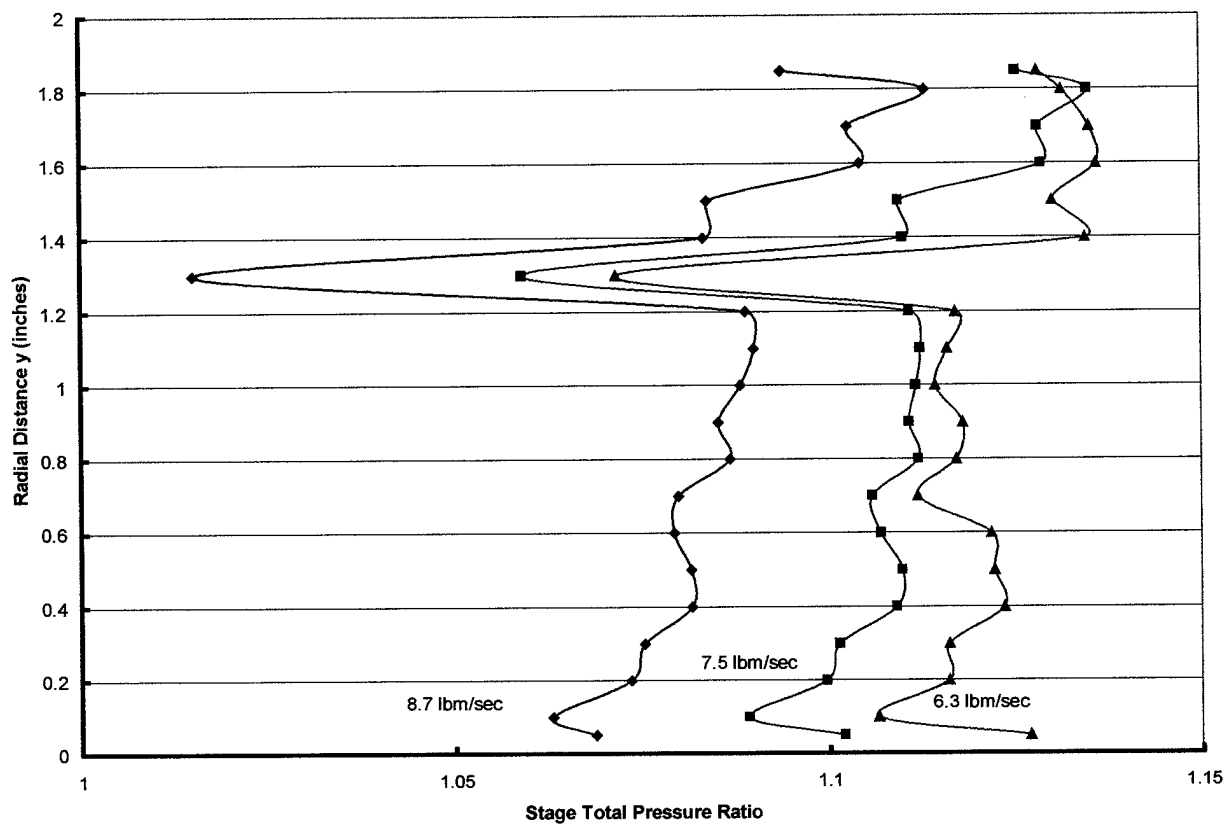
Figure 28.   Exit Stagnation Pressure Distribution at 50% Speed
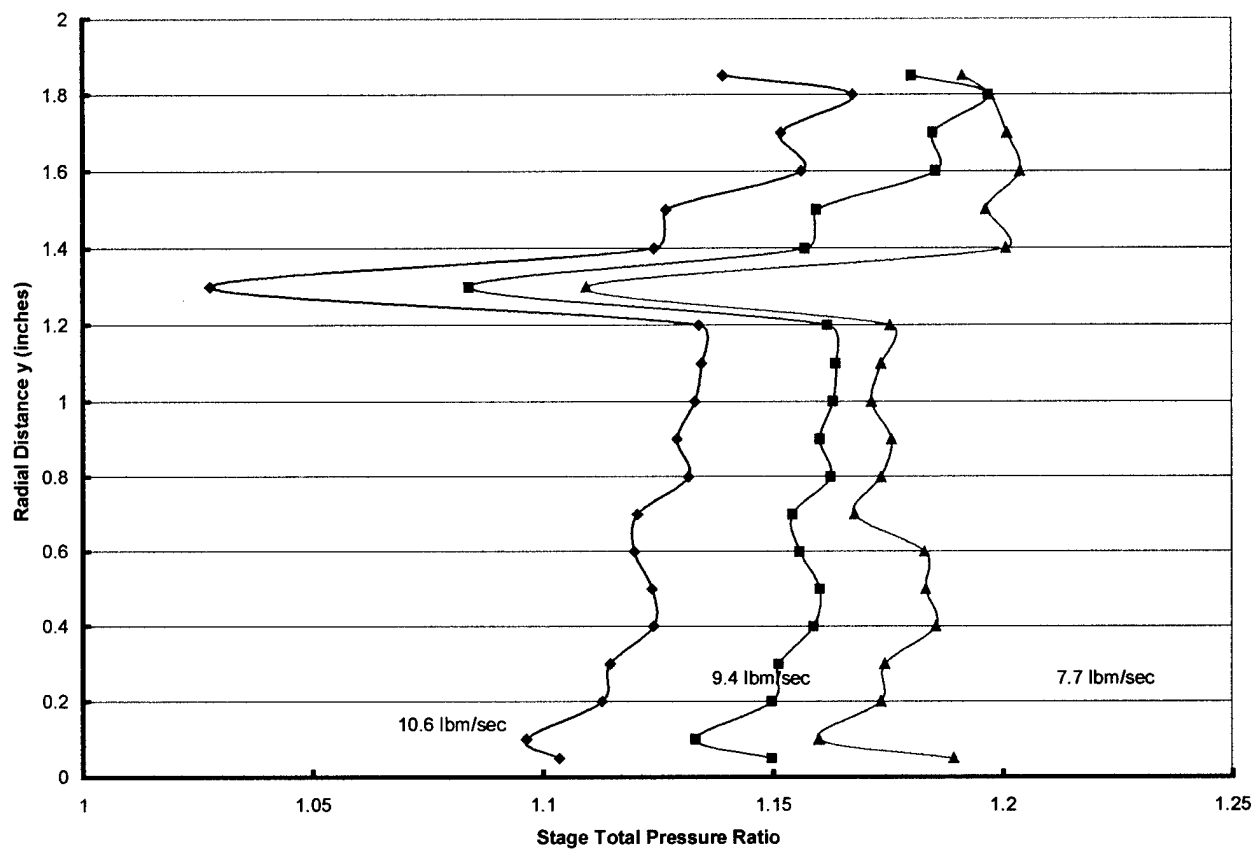
Figure 29.   Exit Stagnation Pressure Distribution at 60% Speed
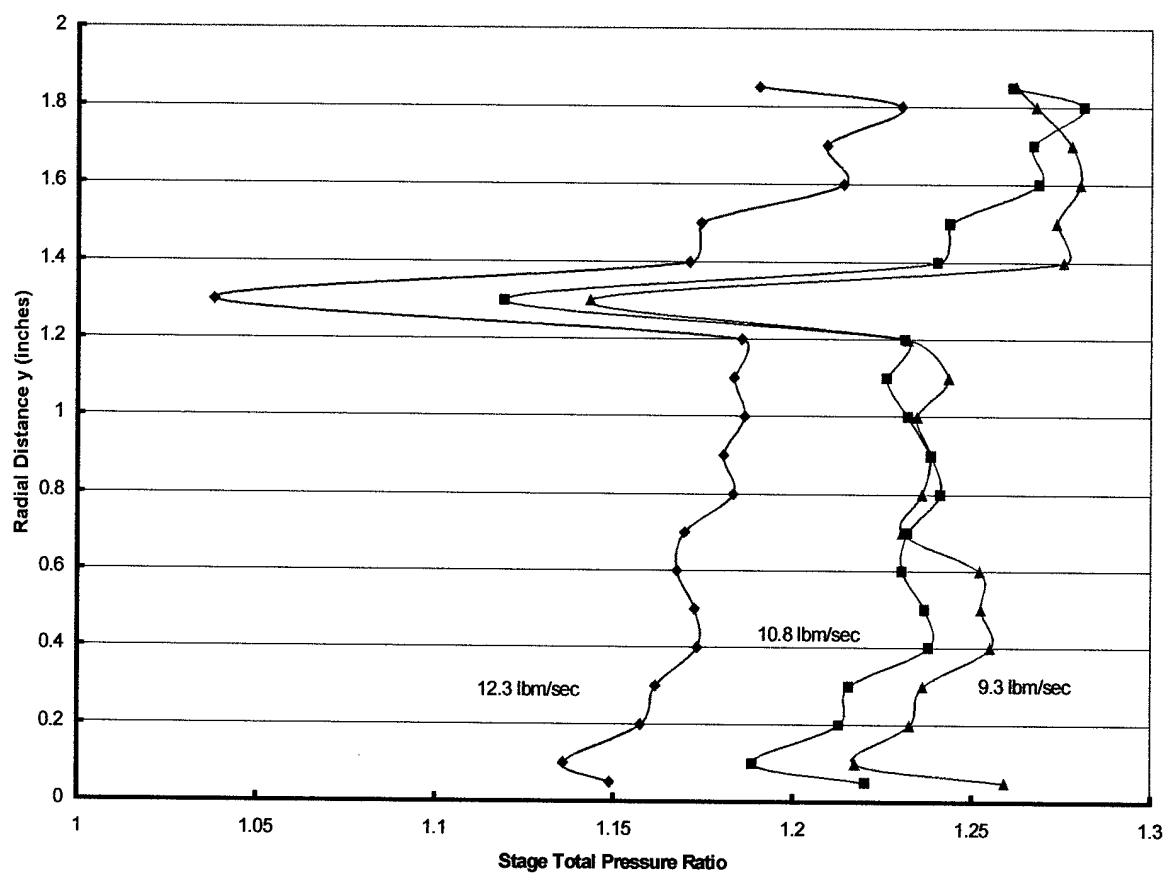
Figure 30.   Exit Stagnation Pressure Distribution at 70% Speed

THIS PAGE INTENTIONALLY LEFT BLANK

V. CONCLUSIONS AND RECOMMENDATIONS

The Transonic Compressor Rig was successfully recommissioned. Improvements were made to the data acquisition systems, monitoring equipment, and data reduction systems. Performance testing of the Sanger stage was conducted up to 70% of the rotor design speed. Testing was halted to make changes based on what was learned before going to higher compressor speeds.

The Plexiglas casewall is an issue that must be addressed before testing is resumed. While the Plexiglas casewall is invaluable (with its transparency, and its ability to withstand contact with the rotor without significant damage to either component), improvements must be made in the way that it is used, or it should be redesigned. It was shown that rotor tip clearances could be controlled by regulating the temperature of the Plexiglas casewall. However, it is necessary to be able to monitor the running tip clearance during testing, in order to adequately determine the effects of casewall temperature on tip clearance, and to control the tip clearance once the effects are known. The conclusion drawn from the present study is that this is both feasible, and desirable.

In the present tests, the torque measurement had too great an uncertainty to allow reliable comparisons to be made between experimental data and performance predictions from Computational Fluid Dynamics. Since the effect of tip clearance on the performance is important in assessing the accuracy of computer modeling, it is important to be certain of the running tip clearance during the tests.

With the experience obtained from the present study, the following specific recommendations are made:

- Improvements in performance data can be obtained by both improving the torque and temperature measurements. A planned modification to the current torque flexure will reduce uncertainties in the torque measurements. A radially distributed temperature probe array across the exit flow will provide a detailed temperature profile for use in determining the mass-averaged temperature rise across the stage.

- Implementation of a method to monitor running tip clearance is essential to achieving the goals of the present program. A running tip clearance measurement would allow the control of tip clearance using casewall temperature.

- The casewall should be redesigned to both implement clearance control and retain the optical access provided by the current Plexiglas design.

LIST OF REFERENCES

1.	Sanger, N.L., <u>Design of a Low Aspect Ratio Transonic Compressor Stage Using CFD Techniques</u>, ASME Journal of Turbomachinery, Vol. 118, 1996.

2.	Grossman, Bart L., <u>Testing and Analysis of a Transonic Axial Compressor</u>, Master's Thesis, Naval Postgraduate School, Monterey, California, September 1997.

3.	Hobson, G.V. (Unpublished) Department of Aeronautics and Astronautics, Naval Postgraduate School, Monterey, CA, April 2000.

4.	United Sensor Corporation, "List Price Schedules", 3 Northern Boulevard, Amherst, NH 03031-2329, April 04, 1994

5.	Avallone, E.A. and Baumeister III, T. (Editors), "Marks Standard Handbook for Mechanical Engineers", Tenth Edition, McGraw-Hill, 1996 (p. 6-188)

6.	von Backström, T.W., Hobson, G.V., Grossman, B.L., and Shreeve, R.P., <u>Investigation of the Performance of a CFD-Designed Transonic Compressor Stage</u>, AIAA Paper 2000-3205, To Be Presented at the 36th AIAA/ASME/SAE/ASEE Joint Propulsion Conference, Huntsville, Alabama, July 17-19, 2000.

7.	Herrmann, Tony, <u>Analysis and Design of the Rotor, Stator, and Nose Cone for the Naval Postgraduate School Transonic Compressor</u>, Engineering Analysis Report, NASA Lewis Research Center, Cleveland, Ohio, February 1994.

8.	ANSYS (version 5.5.1), October 1998

9.	Reid, William D., <u>Transonic Axial Compressor Design Case Study and Preparations for Testing</u>, Master's Thesis, Naval Postgraduate School, Monterey, California, September 1995.

THIS PAGE INTENTIONALLY LEFT BLANK

APPENDIX A   VIBRATIONAL MODES OF THE SANGER ROTOR

A.   EXPERIMENTAL DETERMINATION BY BOWING

Prior to its installation on the test rig, the rotor blades were excited by bowing. A violin bow was used at various points along the free edges of each blade, and the excited frequencies were recorded using the FFT capability of an HP54815A Infinium oscilloscope. A microphone and audio amplifier were used to amplify the tones excited by the bowing, for input to the oscilloscope. Figure A.1 shows the equipment as it was used. After experimenting in how best to excite the pure tones which characterize the lower order modes, the bowing was concentrated at the midpoint of each blade tip, and at the trailing edge of the blade near the tip. The results obtained for the lowest three resonant frequencies (labeled Modes 1-3) are show in Figure A.2.
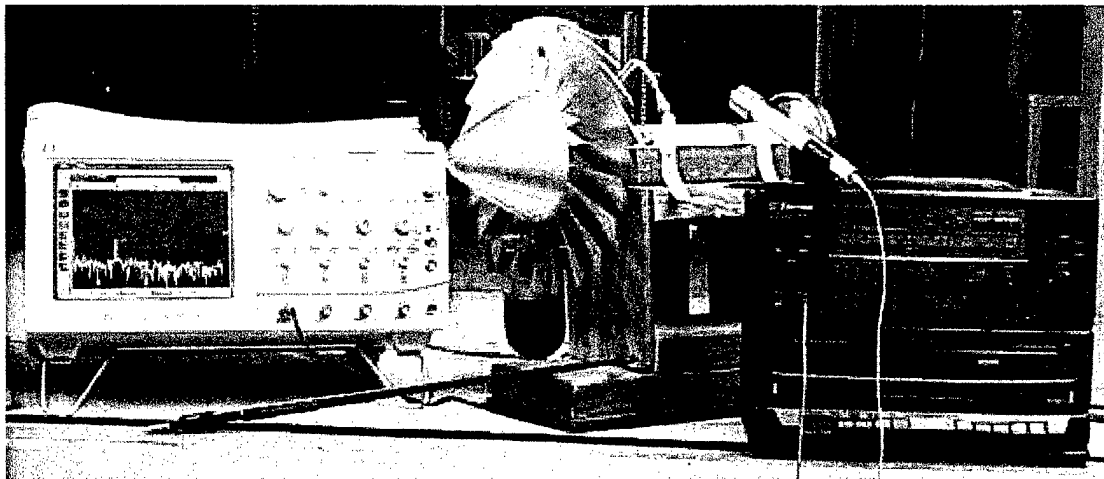
Figure A.1.   Equipment For Detecting Critical Rotor Blade Frequencies

B.   RESULTS OF BOWING

All 22 blades showed similar modal frequencies, with the first mode being detected at approximately 722 Hz, the second at 2664 Hz, and the third at 2794 Hz. These three values compare favorably to the values of 737 Hz, 2697 Hz, and 3053 Hz, calculated using NASTRAN [Ref. 1]. The Campell Diagram [Ref. 7] appears to have incorrectly labeled these modes as 1st Bending, 2nd Bending, and 1st Torsion, respectively. Figure A.2 shows the variation in modal frequency with respect to blade number, and the comparison with the calculated modal frequencies.
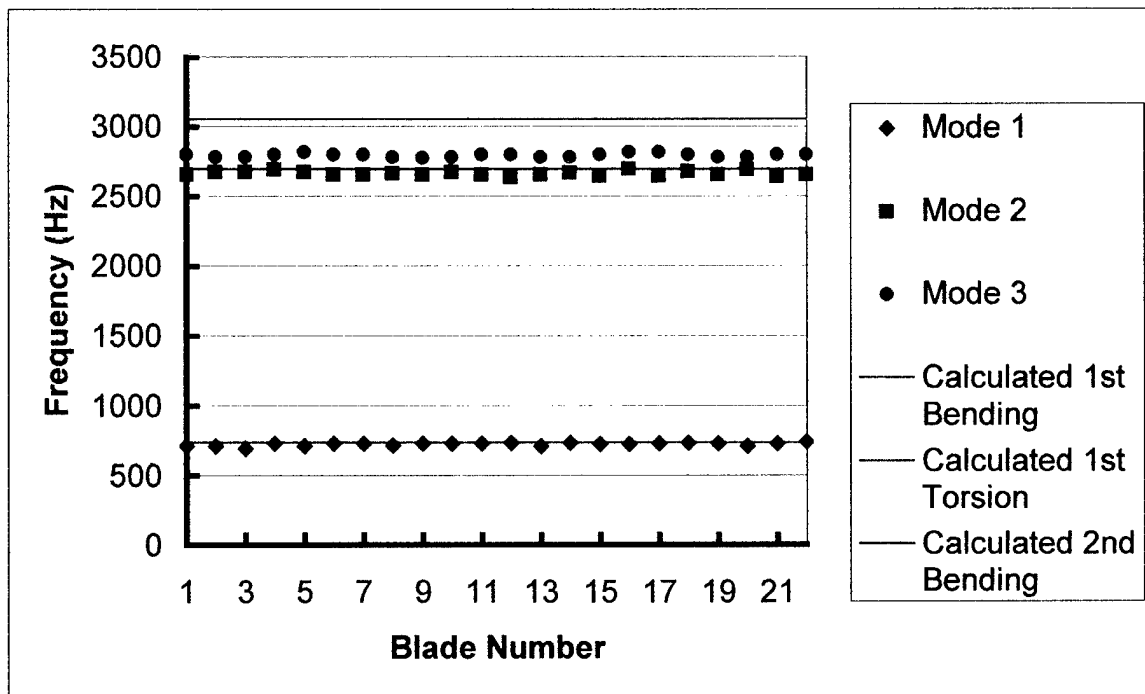
Figure A.2.   Frequency Analysis from Bowing of Blades

C.   COMPARISON WITH COMPUTER-PREDICTED MODES

While distinct blade-vibrational modes were observed, it is difficult to classify them (more particularly the higher order modes) as purely torsional or bending modes. Flat-plate theory does not apply since the thickness of the blade varies and the shape is twisted. The modes of blade vibration exhibit characteristics involving a combination between bending and torsion. The results of an ANSYS simulation [Ref. 8] conducted in-house [Ref. 3] are shown in Figure A.3. The 1st, 2nd, and 3rd modes predicted by the finite element code are seen to be primarily bending, primarily torsion, and a combination of bending and torsion, respectively. The contours in Figure A.3 show the maximum deflections in the blades at these frequencies. The ANSYS simulation did not model the fillet connection to the rotor hub, and assumed an encastered root. In the bowing of the blades, the complete rotor had an effect on the modal frequencies.

| 1st Mode | 2nd Mode | 3rd Mode |
| (746.3 Hz) | (2629 Hz) | (2852 Hz) |
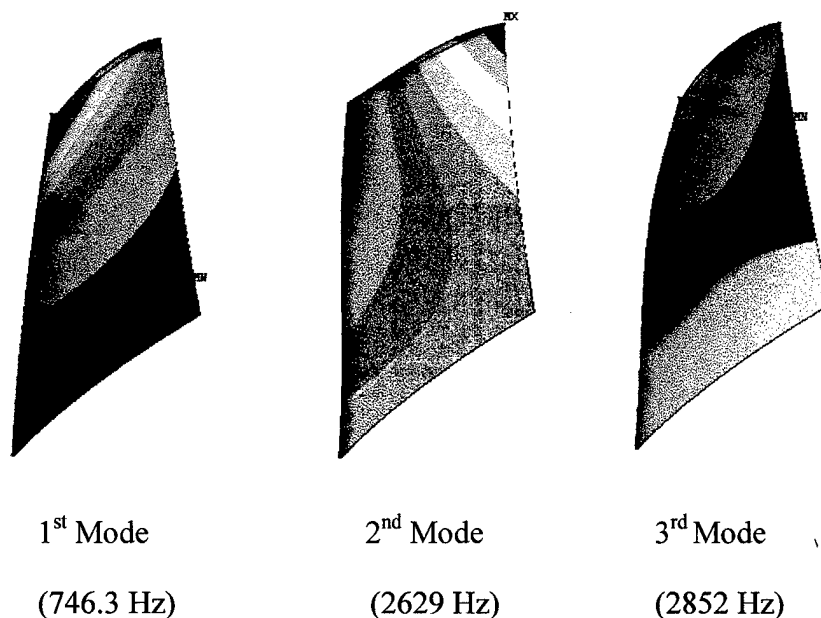
Figure A.3.   Lowest Modes of the Rotor Blades using ANSYS Simulation

THIS PAGE INTENTIONALLY LEFT BLANK

APPENDIX B   CALIBRATION PROCEDURES

Calibration procedures were required for the accurate measurement and recording of torque, and for the instrumentation that was used to control bearing loads and monitor bearing temperatures while testing.

A.   TORQUE CALIBRATION

Torque on the stator, which was free to rotate on bearings, was measured using strain gages on a small beam which opposed the rotational motion [Ref. 9]. A calibration plate was mounted to the stator as shown in Figure B.1, and weights were hung on a 1.44 lb tray hanging from a 20 inch moment arm.
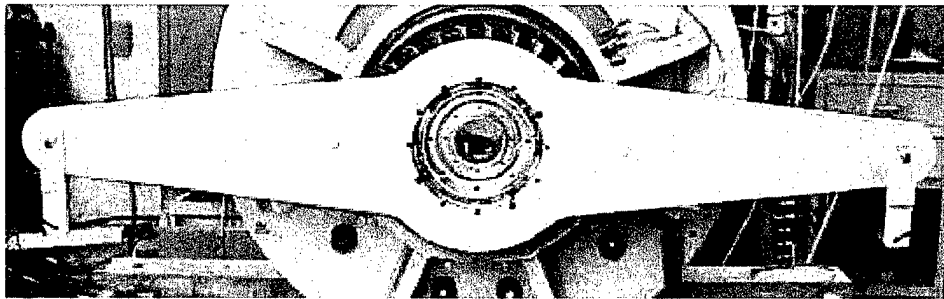
Figure B.1.   Torque Calibration Plate on Stator

HPVEE software was used to collect voltage data while loading and unloading the weights. A plot of the applied torque was generated as a function of strain gauge reading. Figure B.2 shows the data obtained, a polynomial fit through the data, and the resulting calibration coefficients. Reference 9 documents the arrangement and calibration method.
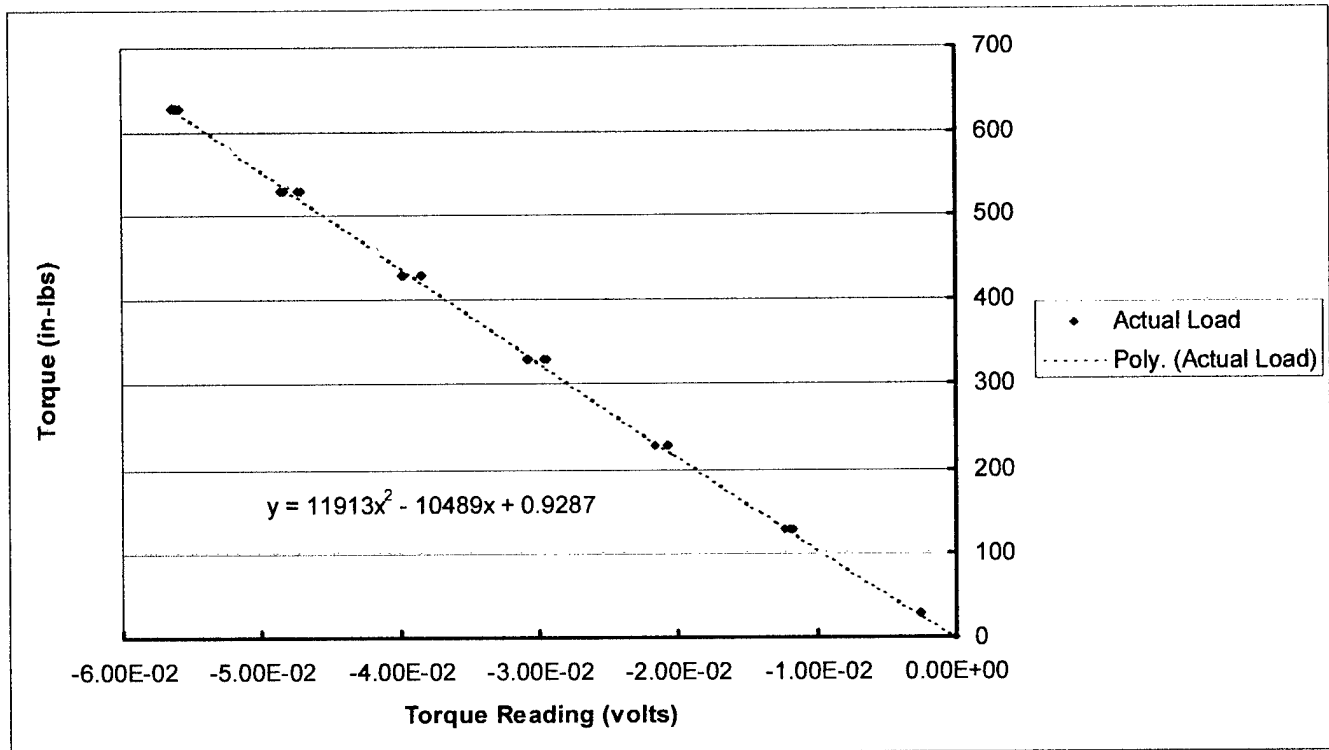
Figure B.2. Torque Calibration Data and Torque Coefficients

B. AXIAL FORCE CALIBRATION

The axial force on the rotor was measured using strain gauges on flexures which held the aft bearings. The axial force information was not required for performance data reduction, but was required in order to monitor and control the axial load on the bearings. Balance air was fed to a balance piston to reduce the axial force on the rotor and assembly, and thereby eliminate unnecessary friction and wear on the bearings.

An initial calibration of the strain gages used in measuring the axial force, was conducted prior to assembly of the compressor rig. This was done by placing weights on

the inner race of the bearing, while holding the strain-gauged flexure horizontally in a frame. The Omega DP25-S Strain Gage Panel Meter was ranged to the maximum applied weight of 30 lbs. Loading and unloading the bearings, provided relatively linear results, validating both the strain gages and the meter. When the rig was fully assembled, a pulley apparatus was set up to provide an axial load to the mounted rotor. Figure B.3 shows the pulley assembly attached to the rotor, with a welded ring on a bolt in place of the spinner retaining bolt.
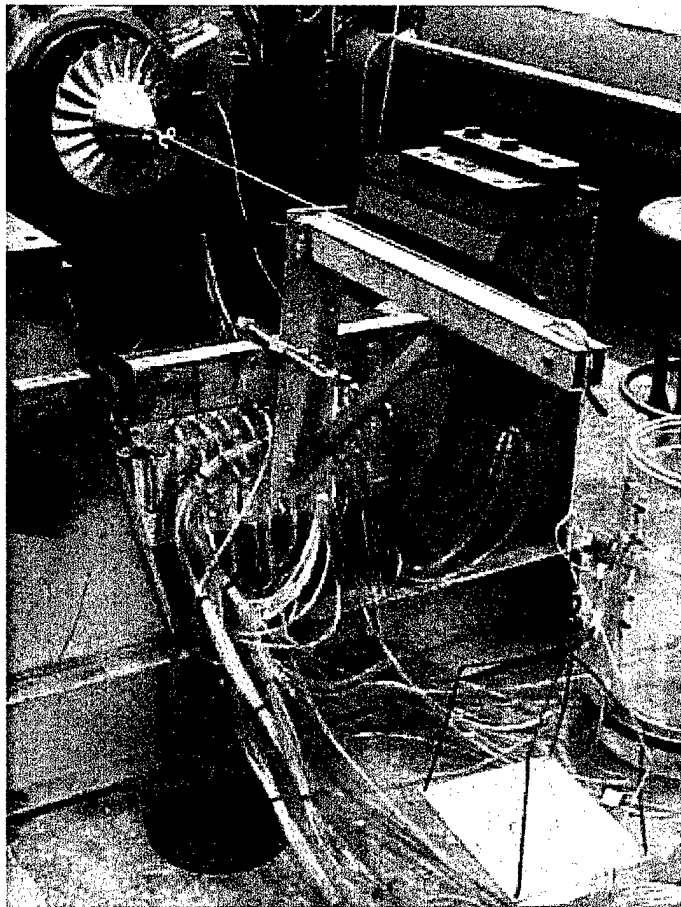
Figure B.3.   Pulley Assembly for Axial Force Calibration

A hanging tray weighing 1.44 lbs was used to apply the axial load to the rotor. The same calibration procedure that was used prior to installing the rotor on the test rig, was repeated. The results are shown in Figure B.4. The non-linear behavior at low axial loads is likely to be the result of friction at the front pair of bearings (between the outer race and containing surface). This interface was designed to slide as the flexures were deflected, and as the drive shaft expanded with an increase in temperature.
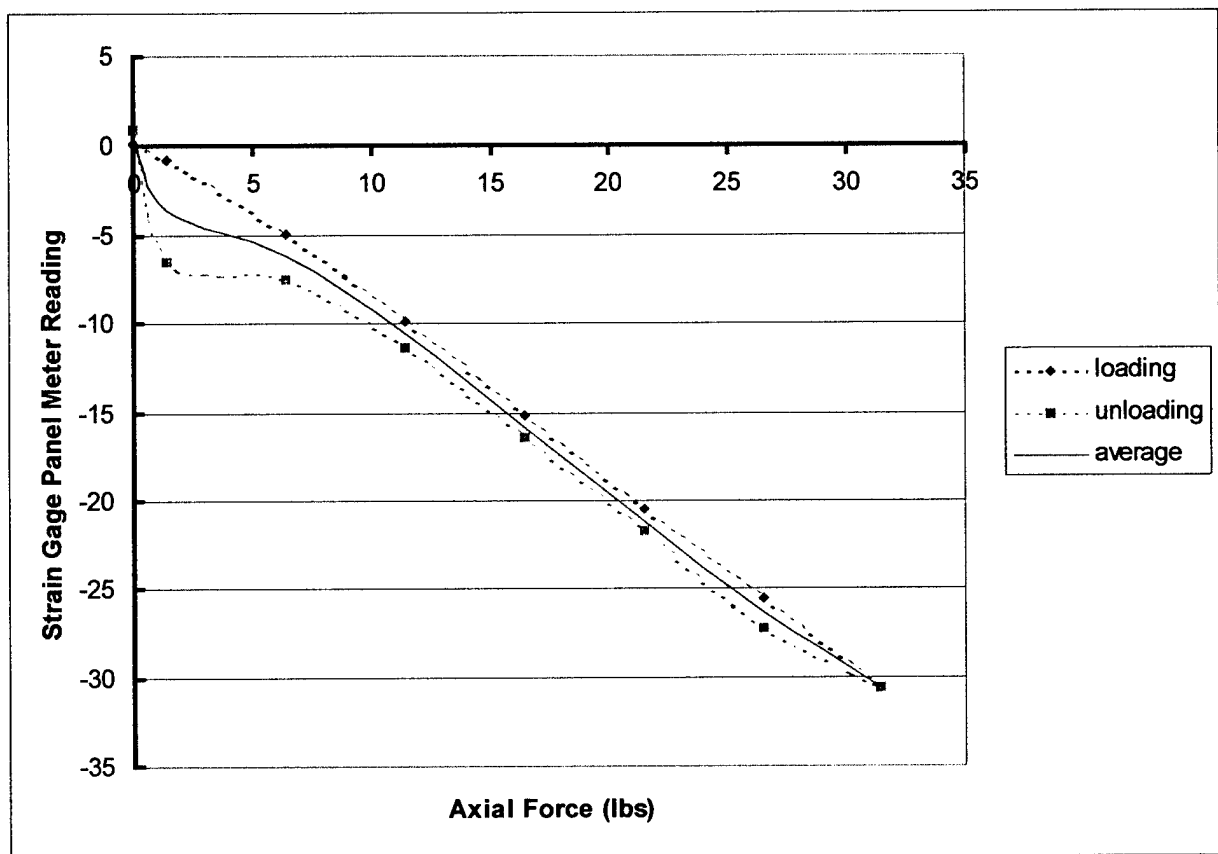
Figure B.4. Strain Gage Panel Meter Readings vs. Actual Axial Force

C. OILERS

The bearing lubrication system for the transonic compressor rig, was an oil mist system. Four separate oilers were used. The operating temperature of the bearings was strongly affected by the air pressure that was set, and by the drop rate of oil into the misters. The air driving the oil misters was taken from the instrument air supply. A regulated air pressure of 40 psia was set, and then the oilers were set for a drop rate of two drops per minute.

D. BEARING TEMPERATURE MONITOR

An Omega 12 Channel Temperature Monitor (Model # CN612TC1) with programmable and scanning capabilities, was used to monitor the bearing temperatures. There were a total of eight bearings, in four matched pairs, in the test rig; a fore and aft bearing pair in the drive turbine, and a fore and aft pair in the test compressor. An iron-constantan contact thermocouple was installed against the outer race of each bearing. Calibration of the monitor was not required. The thermocouple connections were verified prior to testing. Each thermocouple was placed in an ice-bath, and the readings on the thermometer were compared with those displayed by the temperature monitor. The monitor was found to scan properly, and to indicate temperatures correctly within the uncertainty in the temperature of the bath ($\pm 1^{\circ}F$)

The temperature display on the monitor was found to be highly sensitive to noise on input power. An isolation transformer was therefore used to isolate the power supply to the instrument panel.

APPENDIX C   DATA LISTING

The reduced results of all reported runs are listed:

| Point #	% Speed	RPM	Wall Temp 1	Wall Temp 2	Wall Temp	Tip Clearance Static	Blade Extension	Tip Clearance	Referred Mass Flow Rate (lbm/sec)	Pressure Ratio	Adiabatic Efficiency (n1)	Adiabatic Efficiency (n2)	Adiabatic Efficiency (n3)	Referred Torque (in-lbs)	T1	T3	Temp Rise	Referred Horsepower (torque)	Referred Horsepower (temp)
2	50	13573.8	95.1	100.8	97.95	0.01279	6.56E-08	0.01279	8.70463	1.085456	1.012951	1.036959	1.219087	140.0534	71.22	83.64	12.42	29.811246	35.8778758
3	50	13545.1	99.6	102.6	101.1	0.01342	6.55E-08	0.01342	8.212743	1.098057	1.011284	1.032555	1.276707	144.4168	70.76	84.97	14.21	30.688213	38.7426811
4	50	13557	104.6	102.9	103.8	0.01395	6.55E-08	0.01395	7.723143	1.107495	0.982574	1.002934	1.285196	147.0978	69.26	85.2	15.93	31.329616	40.9788126
5	50	13519	110.6	104.9	107.8	0.01475	6.54E-08	0.01475	7.130735	1.116069	0.924095	0.937302	1.251582	150.3792	67.82	86.01	18.19	31.982434	43.3166101
6	50	13592.2	114.9	105.7	110.3	0.01526	6.57E-08	0.01526	6.47327	1.122257	0.832089	0.843722	1.17201	152.5896	69	90.29	21.29	32.591617	45.9057877
7	50	13577	118.3	106.7	112.5	0.0157	6.56E-08	0.0157	6.309427	1.122737	0.778574	0.78902	0.90661	193.2465	69.23	92.07	22.85	41.220857	47.9995629
8	50	13503.1	119	106.4	112.7	0.01574	6.53E-08	0.01574	7.139913	1.116707	0.915082	0.921945	0.994235	190.9105	68.58	87.08	18.5	40.525583	44.0309638
9	50	13563.3	118.6	105.4	112	0.0156	6.56E-08	0.0156	7.548709	1.111719	0.951367	0.964233	1.010951	189.6294	69.38	86.47	17.08	40.402516	42.9329108
10	50	13505.2	116	104.2	110.1	0.01522	6.53E-08	0.01522	7.825328	1.103524	0.988877	1.011512	0.99309	186.625	68.75	84	15.25	39.615713	39.7844684
11	50	13503.9	110.5	102.8	106.7	0.01453	6.53E-08	0.01453	8.161523	1.095043	0.998472	1.024777	0.970004	183.3722	68.12	82.01	13.89	38.944806	37.8344418
12	50	13547.5	94.3	94.9	94.6	0.01212	6.55E-08	0.01212	8.640126	1.086977	0.985913	1.011448	0.970932	177.2586	67.36	80.25	12.89	37.795105	37.2208013
2	60	16269.8	90.8	98.3	94.55	0.01211	7.87E-08	0.01211	10.62393	1.128602	0.997098	1.017256	1.02494	248.5516	58.19	76.45	18.27	64.206378	65.9991942
3	60	16335	99	99.6	99.3	0.01306	7.9E-08	0.01306	10.04602	1.152895	0.991866	1.01062	1.012201	280.4558	61.29	83.08	21.79	72.521715	74.0085844
4	60	16227.7	107.5	101	104.3	0.01405	7.85E-08	0.01405	9.41091	1.162593	0.961753	0.9709	0.973039	291.7425	61.6	85.44	23.84	74.922351	75.8014752
5	60	16349.7	113.1	102.8	108	0.01479	7.9E-08	0.01479	8.776211	1.176073	0.920864	0.934195	0.933184	303.4969	61.18	88.01	26.83	78.558265	79.609236
6	60	16302.3	115.2	103.9	109.6	0.01511	7.88E-08	0.01511	8.01302	1.180182	0.841529	0.862478	0.856512	308.9122	59.36	89.26	29.9	79.868217	81.2902416
7	60	16339	117.2	105.2	111.2	0.01544	7.9E-08	0.01544	7.986799	1.183831	0.796761	0.804973	0.863839	310.9726	61.22	93.51	32.29	80.438245	87.2102837
8	60	16344.9	120.2	107.3	113.8	0.01595	7.9E-08	0.01595	7.727037	1.183607	0.761911	0.774976	0.795639	325.7726	59.99	93.65	33.65	84.395691	88.1316884
9	60	16312.7	120.9	107.5	114.2	0.01604	7.89E-08	0.01604	8.377534	1.177205	0.881061	0.903162	0.853096	319.0814	59.64	87.77	28.12	82.527711	79.908313
10	60	16293.3	120.6	106.8	113.7	0.01594	7.88E-08	0.01594	9.150665	1.169754	0.930623	0.944803	0.914184	312.3048	58.43	83.94	25.51	80.772589	79.3457614
11	60	16256.3	118.2	105.5	111.9	0.01557	7.86E-08	0.01557	9.670756	1.157909	0.958814	0.973455	0.940167	300.555	59.16	82.31	23.15	77.502836	75.9955449
12	60	16234.3	111	103.7	107.4	0.01467	7.85E-08	0.01467	9.941313	1.143966	0.985122	1.010964	0.946361	281.8643	60.61	81.3	20.69	72.483327	69.6313523
13	60	16219.5	103.3	101.8	102.6	0.01371	7.84E-08	0.01371	10.52582	1.129983	0.987117	1.007813	0.950136	269.3099	58.58	77.23	18.65	69.327522	66.7302876
3	70	18928	97.2	100.6	98.9	0.01298	9.15E-08	0.01298	12.31085	1.178553	0.987075	1.014764	2.87E-78	1.21E+80	62.14	87.54	25.41	3.626E+79	105.566501
4	70	19024.7	101.4	105.2	103.3	0.01386	9.2E-08	0.01386	11.74879	1.210637	0.98565	1.002439	3.04E-78	1.27E+80	63.29	93.07	29.78	3.817E+79	117.842825
5	70	19043.9	114.9	109.6	112.3	0.01565	9.21E-08	0.01565	10.80377	1.237501	0.948502	0.962686	0.908714	437.9867	65.97	100.8	34.79	131.44953	125.935429
6	70	19102	120.3	120.6	120.5	0.01729	9.24E-08	0.01729	9.705313	1.253251	0.817364	0.82612	0.89254	423.8569	66	108.8	42.85	127.59272	139.327931
7	70	18890.2	128.3	122.3	125.3	0.01826	9.13E-08	0.01826	9.319334	1.251454	0.763773	0.768634	0.911668	398.9984	62.63	107.9	45.26	119.16042	142.234217
8	70	18929	129.9	121.7	125.8	0.01836	9.15E-08	0.01386	9.910794	1.239028	0.902282	0.926698	0.920976	400.36	63.71	100.3	36.63	119.68909	122.168891
9	70	18973.5	129.8	118.6	124.2	0.01804	9.17E-08	0.01804	11.39279	1.219508	0.840936	0.963552	0.920598	423.512	61.7	93.74	32.05	127.15352	123.330419
10	70	19059.4	127.2	111.7	119.5	0.01709	9.21E-08	0.01709	11.97544	1.2018	0.974582	0.995504	0.941138	400.7917	61.94	90.8	28.86	120.84805	116.700949
11	70	18850.1	108.7	101.5	105.1	0.01422	9.11E-08	0.01422	12.19131	1.175847	0.976152	0.998951	0.926758	367.4658	60.34	85.58	25.23	109.75143	104.197866
1	70	19042.9	101.2	97.3	99.25	0.01305	9.21E-08	0.01305	12.35484	1.177546	0.99621	1.020216	0.96052	361.8783	68.97	94.33	25.37	108.29314	104.413468
2	70	19019.7	101.2	97.3	99.25	0.01305	9.2E-08	0.01305	12.29699	1.177813	0.99247	1.024588	0.925843	373.8786	66.76	92.15	25.39	111.98212	104.464514
3	70	18958.2	101.2	97.3	99.25	0.01305	9.17E-08	0.01305	12.36501	1.179056	1.002607	1.02758	0.941526	372.9273	65.63	90.88	25.25	111.45608	104.665977
4	70	18961.4	112.9	99.7	106.3	0.01446	9.17E-08	0.01446	11.11339	1.22723	0.955607	0.967036	0.987814	398.5053	63.34	96.32	32.97	119.38072	123.404178
5	70	19025.2	112.9	99.7	106.3	0.01446	9.2E-08	0.01446	11.0167	1.22788	0.952544	0.966123	0.972657	401.9928	66.16	99.51	33.35	120.50604	123.050576
6	70	18891	112.9	99.7	106.3	0.01446	9.18E-08	0.01446	11.12627	1.226764	0.952315	0.968743	0.961241	409.5854	65.93	99.12	33.19	122.58844	123.737413
7	70	18931.6	122.2	105.7	114	0.01599	9.17E-08	0.01599	10.39638	1.241772	0.905489	0.920128	0.883615	441.7607	62.36	99.15	36.79	132.25519	129.06018
8	70	19025.7	122.2	105.7	114	0.01599	9.2E-08	0.01599	10.46018	1.24285	0.908936	0.916451	0.926963	423.8324	63.59	100.5	36.89	127.36842	129.894561
9	70	19018.2	122.2	105.7	114	0.01599	9.19E-08	0.01599	10.43869	1.24317	0.912542	0.920235	0.916879	428.8659	64.96	101.9	36.89	128.66164	129.273129
10	70	18962.6	123.7	107.3	115.5	0.0163	9.17E-08	0.0163	9.586601	1.250465	0.801166	0.807128	0.861786	432.5915	66.58	109.9	43.32	129.20101	138.976893
11	70	18958.2	125.55	109.9	117.7	0.016745	9.17E-08	0.016745	9.526919	1.250418	0.798025	0.806512	0.841346	439.8205	65.27	108.6	43.37	131.49331	138.631368
12	70	19014	127.4	112.5	120	0.01719	9.19E-08	0.01719	9.492056	1.249289	0.789983	0.79871	0.860196	427.8043	70.8	114.9	44.09	127.60674	138.948214
13	70	18989.6	128.9	117.6	123.3	0.01785	9.18E-08	0.01785	9.683374	1.251349	0.783839	0.79473	0.839837	449.4041	67.05	111.5	44.46	134.35307	143.95133
14	70	18948.7	128.1	117.25	122.7	0.017735	9.16E-08	0.017735	9.5109	1.250567	0.799061	0.804733	0.845587	438.8594	68.94	112.6	43.64	130.6842	138.293546
15	70	18999.7	127.3	116.9	122.1	0.01762	9.19E-08	0.01762	9.571186	1.251444	0.780389	0.794418	0.836354	444.4786	63.54	107.9	44.37	133.39625	142.96274
16	70	18973.2	104.8	97.1	101	0.01339	9.17E-08	0.01339	9.389238	1.252675	0.771849	0.78465	0.864069	426.9822	69.57	115.2	45.59	127.23645	142.438649
17	70	19062.5	105.95	98.7	102.3	0.013665	9.22E-08	0.013665	9.396145	1.254695	0.760434	0.769834	0.865481	426.385	66.23	112.5	46.32	126.06114	145.751618
18	70	19020.4	107.1	100.3	103.7	0.01394	9.2E-08	0.01394	9.334791	1.253615	0.759209	0.766492	0.840352	436.3773	68.3	114.7	46.39	130.51577	144.465178
19	70	18957.9	110.2	104.3	107.3	0.01465	9.17E-08	0.01465	10.83629	1.2355	0.927071	0.941824	0.899385	440.9124	62.47	97.55	35.08	132.17054	128.223418
20	70	18942.6	109.9	104.15	107	0.014605	9.16E-08	0.014605	11.02073	1.234183	0.939564	0.950818	0.935021	430.5077	65.09	99.7	34.61	128.62523	128.003331
21	70	18965.7	109.6	104	106.8	0.01456	9.17E-08	0.01456	10.85887	1.23417	0.944296	0.957982	0.899295	441.0403	66.43	101	34.52	131.76394	125.484654
22	70	18920.9	108.1	102.2	105.2	0.01423	9.15E-08	0.01423	11.66341	1.200986	0.974338	1.000001	0.90111	409.666	63.34	92.18	28.84	122.46241	113.258587
23	70	18908.1	106.7	100.65	103.7	0.013935	9.14E-08	0.013935	11.8601	1.200552	0.984346	1.002738	0.920465	407.9844	65.19	93.77	28.59	121.66195	113.766374
24	70	18920.6	105.3	99.1	102.2	0.01364	9.15E-08	0.01364	11.84886	1.199874	0.975908	0.997904	0.914002	408.8231	64.97	93.7	28.73	122.01814	114.277972

71

THIS PAGE INTENTIONALLY LEFT BLANK

APPENDIX D   DATA ACQUISITION PROGRAMS

The operating procedure for using the HPVEE data acquisition program can be found in Reference 2.

In the following pages, which document the program, each HPVEE subprogram is listed following the HPVEE graphical description.
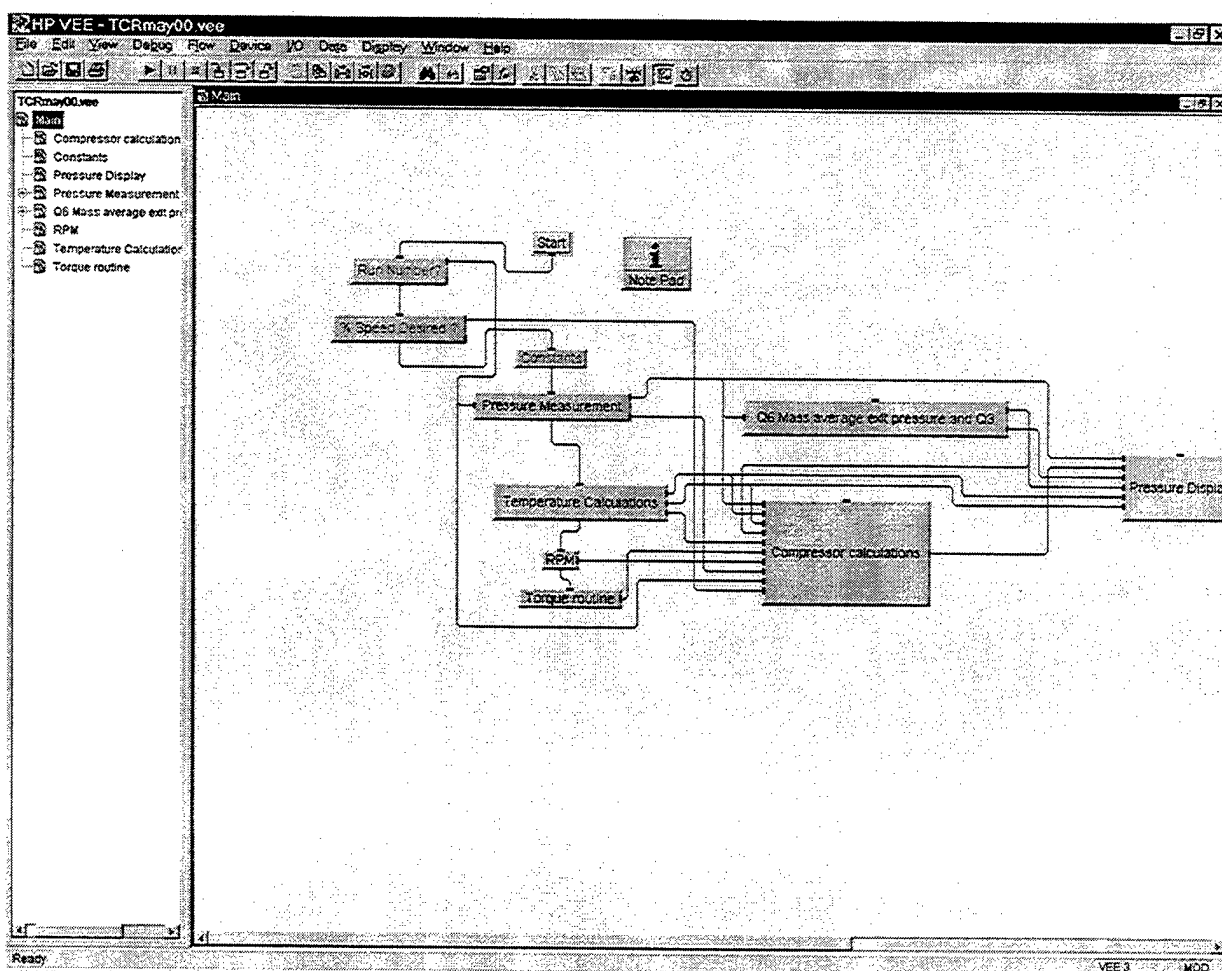
Compressor Calculations

Inputs: Pressure (array)   temp   speed
        T1   Torque   run
        T3   RPM
        Q6   Patm

Constants Used:
     AO   CO
     gamma1

Equations

$B0 = (32.172 * pinf * AO)/(gamma1 * VO * W2 * 2.036)$

$D2 = T3 - T1$

$Delta = Q1/\text{Reference Pressure}$

$E0 = S3 * (2 * B0 * X0 * Y3^{gamma1-1}) * U2/U1$

$E1 = (Y1^{gamma1-1}) * S3$

$E2 = (Y2^{gamma1} * B0 * X0 - 1) * S3$

$E3 = E1 * U2/U1$

$Pinf = pressure[48]$

$Q1 = (pressure[5] + pressure[6])/2$

Reference Pressure = 29.920

Reference Temperature = 518.670

Referred Flow = $W2 * sqrt(theta)/delta$

Referred Horsepower 1 = $U1/(sqrt(theta) * delta)$

Referred Horsepower 2 = $U2/(sqrt(theta) * delta)$

Referred Speed = $RPM/theta$

Referred Torque = $Torque/delta$

$S3 = (T1 + 459.67)/D2$

Theta = $(T1 + 459.67)/\text{Reference Temperature}$

$U1 = 0.000015865 * torque * RPM$

$U2 = 0.33957 * W2 * D2$

$VO = 109.62 * sqrt(T1 + 459.67)$

$W2 = 16.5424 * (1 - (0.039346 * drop)/pressure[3]) * CO * sqrt((pressure[3] * drop)/(T1 + 459.67))$

$X0 = sqrt(B0^2 + 1) - B0$

$Y1 = Q6/Q1$

$Y2 = Q6/Pinf$

$Y3 = Patm/Pinf$

	reduced		raw
now()		now()	
W2		pressure	
Referred Flow		temp	
U1		T1	
Referred Horsepower 1		T3	
U2		Q1	
Referred Horsepower 2		Q6	
Referred Speed		Torque	
Referred Torque		RPM	
E0		Patm	
E1		run	
E2		speed	
E3			
Run			
speed			

Outputs:

The four data files "reduced (total)", "reduced (individual)", "raw (total)" and "raw (individual)"
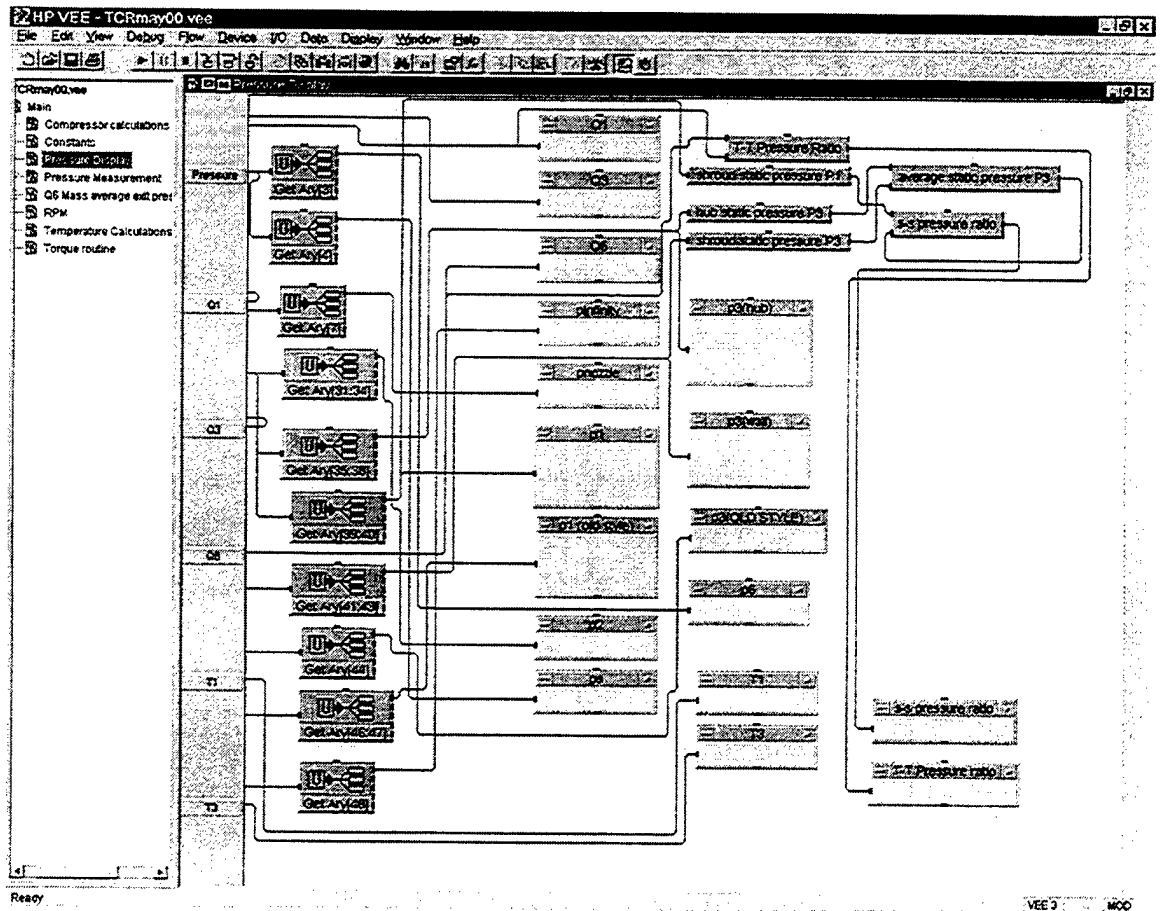Q1
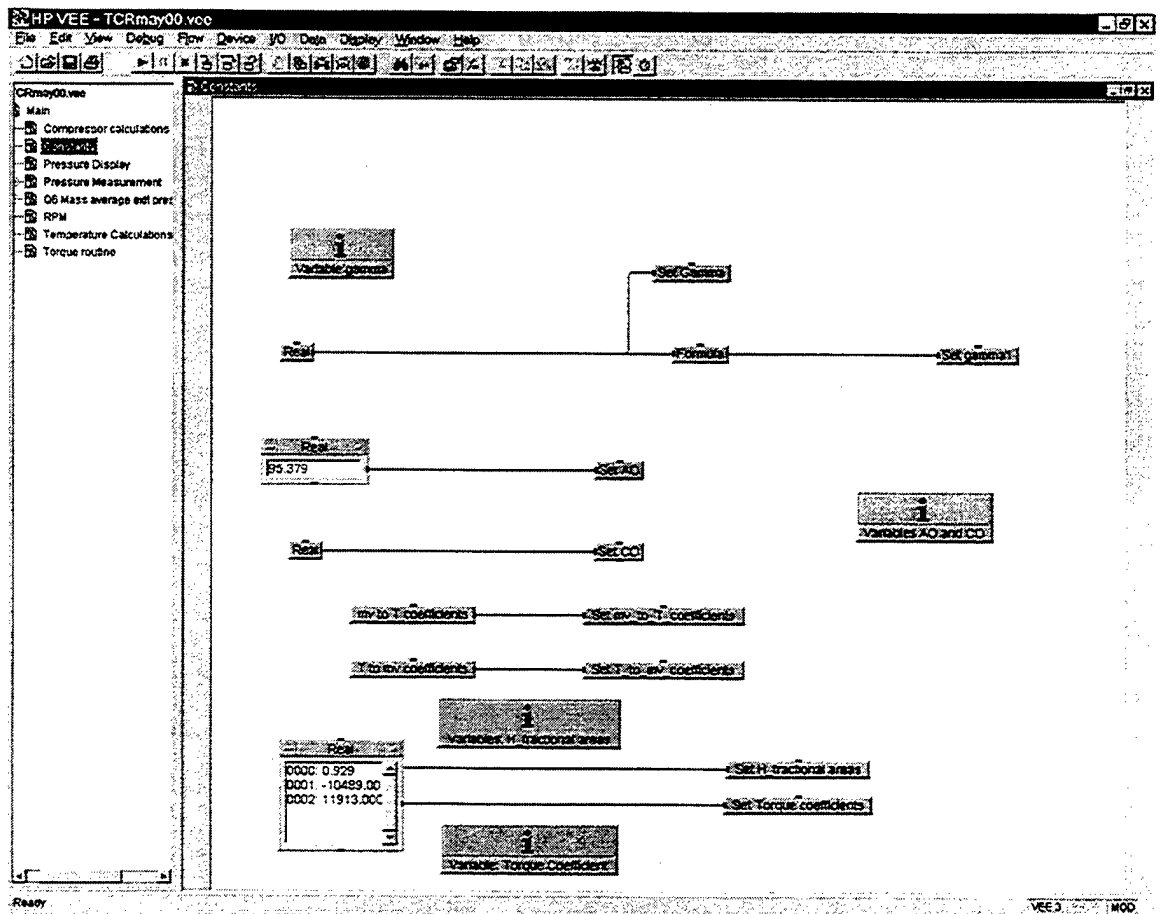
Constants

Inputs: The values for the constants

Equations: Assigning the values for different constants

gamma1=(gamma-1)/gamma

Outputs:	AO
	CO
	H_fractional_areas
	Torque_coefficients
	mv_to_T_coefficients
	T_to_mv_coefficients
	gamma
	gamma1

Pressure Display

Inputs: Pressure (array)   Q6
           Q1   T1
           Q3   T3

Equations:

T-T pressure ratio = Q6/Q1
shroud static pressure P1= mean (pressure[39:40])
hub static pressure P3 = mean (pressure[35-38])
shroud static pressure P3 = mean (pressure [41:43])
average static pressure P3 = (hub static pressure P3 + shroud static pressure P3)/2
s-s pressure ratio = average static pressure P3/shroud static pressure P1

Displays:

s-s pressure ratio	
T-T pressure ratio	
p3 (hub)	(pressure[35-38])
p1	(pressure[39:40])
p2	(pressure[31:34])
p1 (old style)	(pressure[46:47])
p3 (wall)	(pressure[41:43])
p3 (old style)	(pressure[44])
p6	(pressure[3])
ps	(pressure[4])
pnozzle	(pressure[7])
pinfinity	(pressure[48])
Q1	
Q3	
Q6	
T1	
T3	
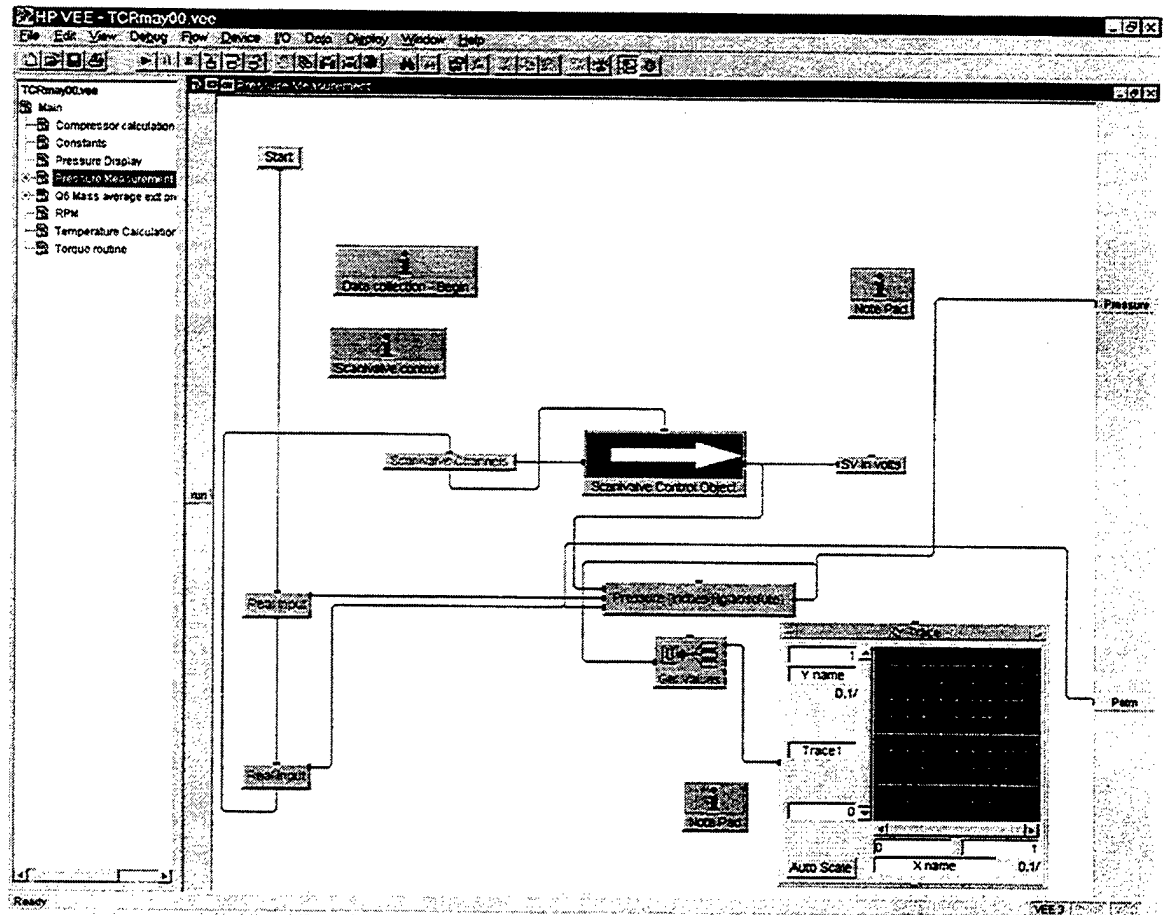
Pressure Measurement

Input:
Start command
Scanivalve Channels (a definition of which channels are to be checked, located in this subroutine)

Prompted Input:
Calibration Pressure in inches of Hg gage; "gage"
Ambient Pressure in inches of Hg absolute; "Patm"

Constants Used:
gamma
H_fractional_areas

Equations:
Subroutine **Scanivalve Control Object**
Inputs: Scanivalve Channels
Equations:
Various procedures to determine which ports need to be checked, step through them, and collect data from them for each of the four scanivalves.
Output: SV (in volts) - This is the data from the scanivalves, in an array

Pressure (inches Hg absolute) = $(SV-SV[1])*(gage/(SV[2]-SV[1]))+Patm$

Outputs:
Patm
Pressure (array)

Displays:

Pressure (inches Hg absolute) is plotted (11:30 the Kiel Probes) in an XY trace

Q6 Mass average exit pressure and Q3

Input: Pressure

Constants Used:
> gamma
> H_fractional_areas

Equations:
> Subroutine **P3**
> **Inputs:** Pressure
> **Equations:**
>> Hub static pressure station 3 = mean (pressure[35:38])
>> Shroud static pressure station 3 = mean (pressure[41:44])
>> Static pressure station 3 = (shroud static pres. station 3 +hub static pres. station 3)/2
> **Output:** Static pressure station 3

Formula1 (array of 20) = ((1/(Total/static)(i))^(1/gamma))*
$\qquad\qquad\qquad$ sqrt(1-(1/(Total/static)(i))^((gamma-1)/gamma))* (Total/static)(i)
Formula2 (array of 20) = (Total/static)(i)*Formula1(i)*H_fractional_areas(i)
Formula3 (array of 20) = Formula1(i)*H_fractional_areas(i)
Q6 = Sum1(x)/Sum2(x) * static pressure station 3
Q3 = mean (Total/static[1:20])
Sum1(x) = Sum Formula2(i) for i = 1:20
Sum2(x) = Sum Formula3(i) for i = 1:20
Total/static (array of 20) = pressure(11:30)/static pressure station 3

Outputs:
Q3
Q6
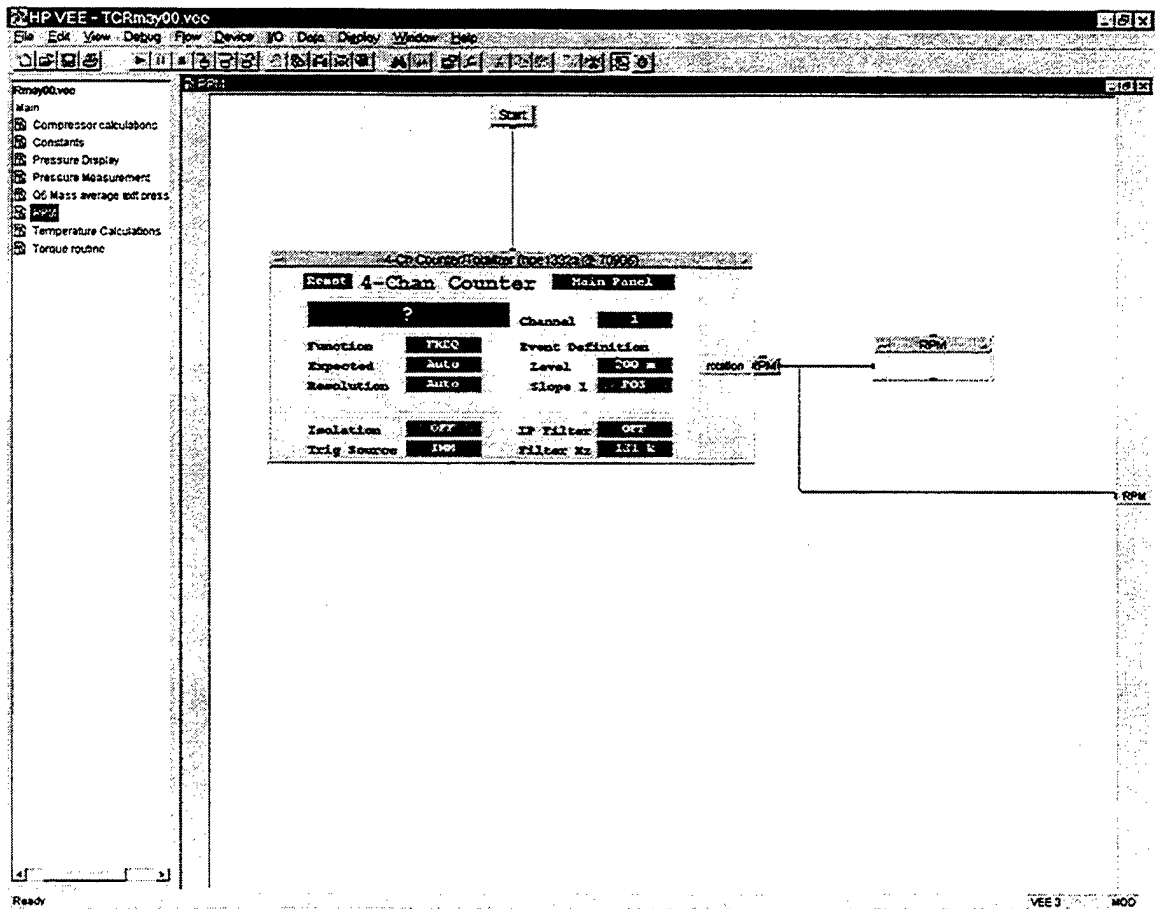
RPM

Inputs: Data from the 4 channel Counter/Totalizer (hpe 1332a @70906)

Equations:

The 4 channel counter/totalizer provides a reading of the rotational speed, given as "rotation"

RPM = rotation * 10

Output:

RPM
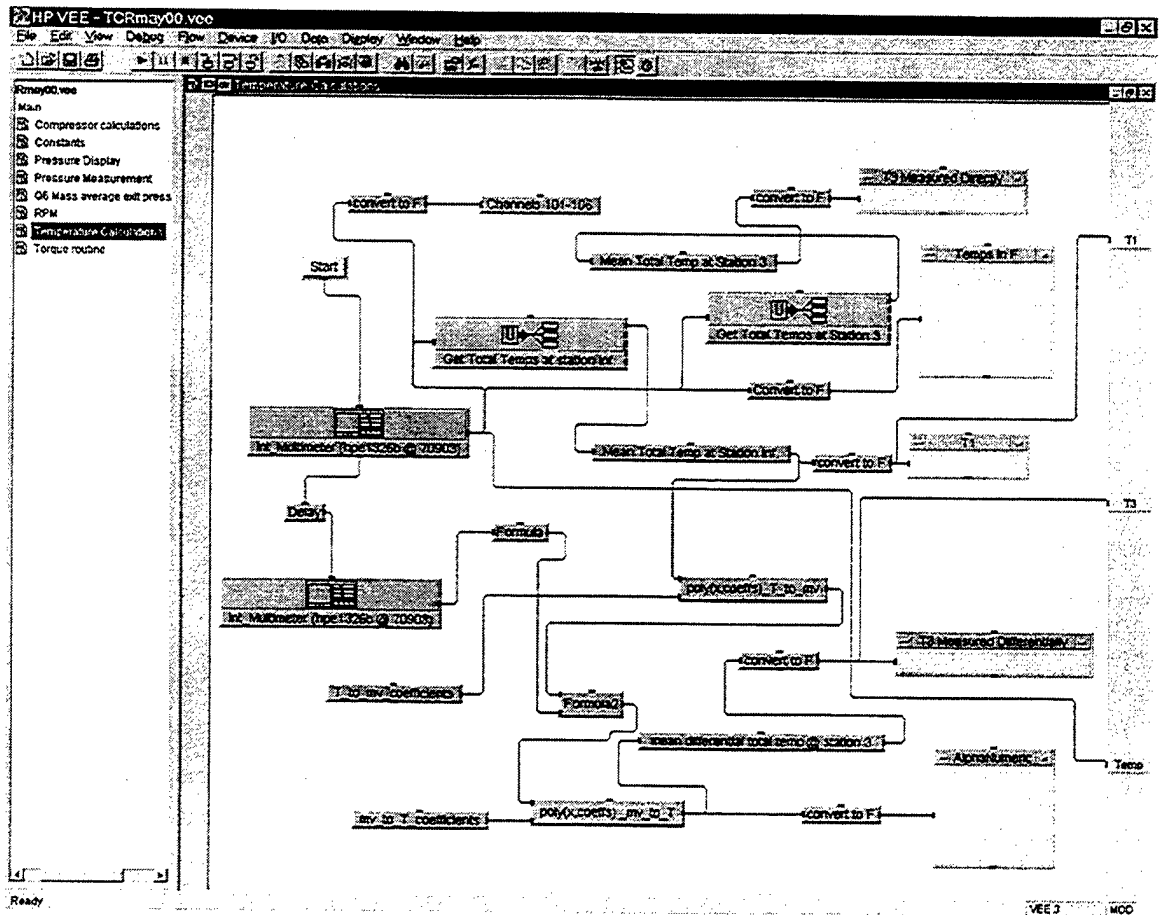
Temperature Calculations

Inputs:

Start command
Data from the Int_Multimeter (hpe1326b @ 70903)
Channel 01 = T_t Station Inf @ 3 o'clock
Channel 02 = T_t Station Inf @ 9 o'clock
Channel 03 = T_t Station 3 Probe 21
Channel 04 = T_t Station 3 Probe 22
Channel 05 = T_t Station 3 Probe 23
Channel 10 = ΔT_t Station Inf @ 3 o'clock and probe 21
Channel 11 = ΔT_t Station Inf @ 3 o'clock and probe 23

Constants Used:

T_to_mv_coefficients
mv_to_T_coefficients

Equations:

The Int_Multimeter reads channels 101-106 and assigns those values to "readings1"
The Int_Mulitmeter reads channels 111-112 and assigns those values to "readings2"

Convert to F , multiplies temperatures by 9/5, and then adds 32
Formula(i) = -readings2(i)*1000
Formula2 = Formula+poly(x,coeffs)_T_to_mv
Mean Total Temp at Station Inf. = mean (readings1[0:1])
Mean Total Temp at Station 3 = mean (readings1[2:4]
Mean differential total temp @ station 3 = mean (poly(x,coeffs)_mv_to_T)
poly(x,coeffs)_T_to_mv =poly(Mean Total Temp at Station Inf.,T_to_mv_coefficients)
poly(x,coeffs)_mv_to_T =poly(Formula2,T_to_mv_coefficients)

T1 = Mean Total Temp at Station Inf. (in degrees F)
T3 = mean differential total temp @ station 3 (in degrees F)
Temp = readings1

Outputs:

T1
T3
Temp

Displays:

Channels 101-106 in degrees F
Poly(x,coeffs)_mv_to_T in degrees F
T1 in degrees F
T3 Measured Directly in degrees F
T3 Measured Differentially in degrees F
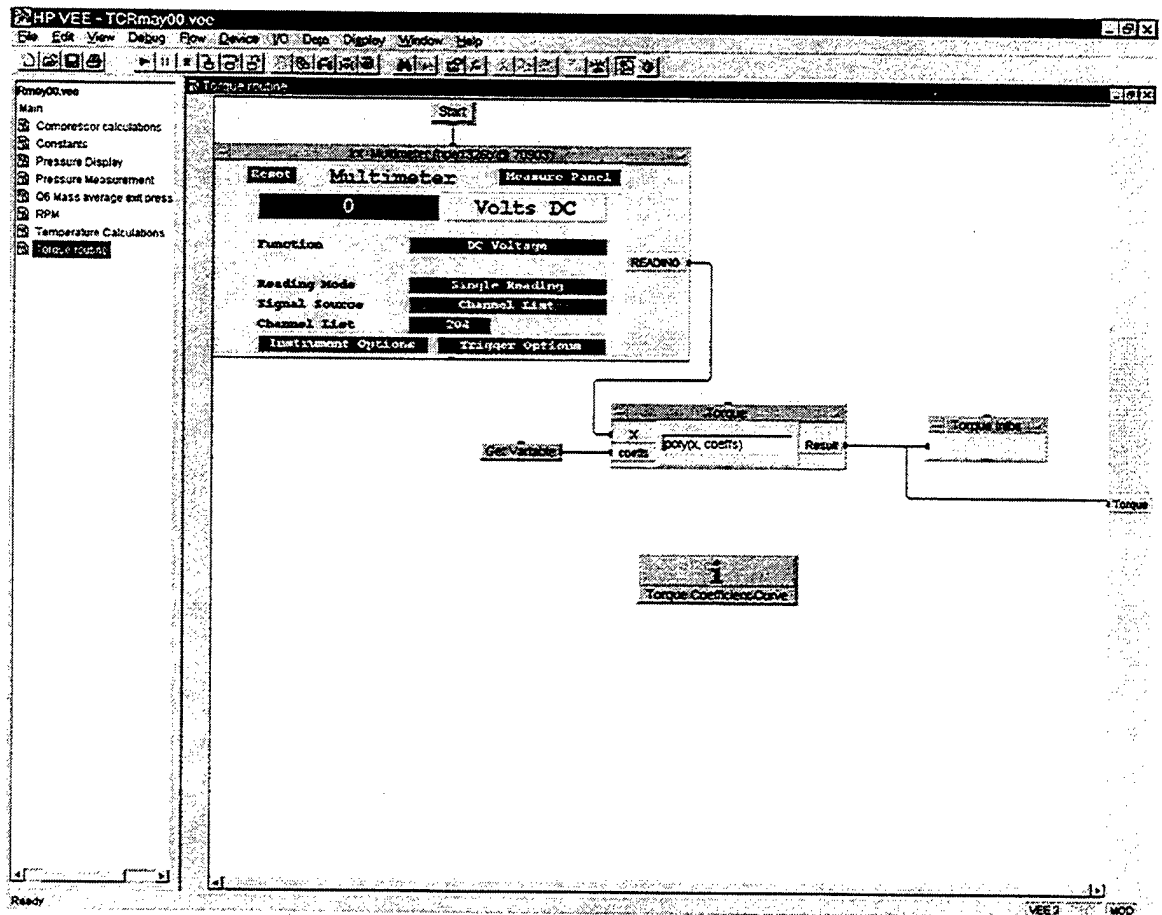
Torque Routine

Inputs: Data from the Int_Mulitmeter (hpe1326b @ 709303) (channel 204)

Constants Used:
        Torque_coefficients

Equation:

The Int_Multimeter provides a reading of the torque, given as "reading"
Torque = poly(reading,Torque_coefficients)

Output:

Torque (in-lbs)

Display:

Torque (in-lbs)

THIS PAGE INTENTIONALLY LEFT BLANK

INITIAL DISTRIBUTION LIST